SOLAR – AIDED LIMESTONE CALCINED CLAY CEMENT PRODUCTION

A THESIS SUBMITTED TO
THE GRADUATE SCHOOL OF NATURAL AND APPLIED SCIENCES
OF
MIDDLE EAST TECHNICAL UNIVERSITY

BY

KAĞAN BERKAY YÖRÜK

IN PARTIAL FULFILLMENT OF THE REQUIREMENTS
FOR
THE DEGREE OF MASTER OF SCIENCE
IN
CIVIL ENGINEERING

SEPTEMBER 2026

Approval of the thesis:

SOLAR – AIDED LIMESTONE CALCINED CLAY CEMENT PRODUCTION

submitted by **KAĞAN BERKAY YÖRÜK** in partial fulfillment of the requirements for the degree of **Master of Science** i**n Civil Engineering, Middle East Technical U**niversity by,

Prof. Dr. Naci Emre Altun
Dean, **Graduate School of Natural and Applied Sciences** _____

Prof. Dr. Erdem Canbay
Head of the Department, **Civil Engineering** _____

Assoc. Prof. Dr. Çağla Meral Akgül
Supervisor, **Civil Engineering, METU** _____

Examining Committee Members:

Prof. Dr. İsmail Özgür Yaman
Civil Engineering Dept., METU _____

Assoc. Prof. Dr. Çağla Meral Akgül
Civil Engineering Dept., METU _____

Assoc. Prof. Dr. Hande Işık Öztürk
Civil Engineering Dept., METU _____

Assoc. Prof. Dr. Onur Taylan
Mechanical Engineering Dept., METU _____

Prof. Dr. Can Baran Aktaş
Civil Engineering Dept., Başkent University _____

Date: 04.09.2026

I hereby declare that all information in this document has been obtained and presented in accordance with academic rules and ethical conduct. I also declare that, as required by these rules and conduct, I have fully cited and referenced all material and results that are not original to this work.

Name Last name : Kağan Berkay Yörük

Signature :

ABSTRACT

SOLAR – AIDED LIMESTONE CALCINED CLAY CEMENT PRODUCTION

Yörük, Kağan Berkay
Master of Science, Civil Engineering
Supervisor : Assoc. Prof. Dr. Çağla Meral Akgül

September 2026, 85 pages

The cement industry is a major contributor to global carbon dioxide (CO_2) emissions due to the energy- and carbon-intensive production of Portland cement clinker. Limestone calcined clay cement (LC^3) offers a lower-carbon alternative by partially replacing clinker with calcined clay and limestone. This study investigated the promising results of using solar-calcined clay in LC^3, with conventionally furnace-calcined clay serving as a laboratory reference.

A locally sourced kaolinite–alunite clay was calcined using a high-flux solar simulator coupled with a rotary reactor and a laboratory muffle furnace at nominal temperatures of 550–800 °C for holding periods of 0.5 and 2 h. The mineralogical and thermal changes induced by calcination were examined using X-ray diffraction (XRD) and thermogravimetric analysis with derivative thermogravimetry (TGA/DTG). Gaussian deconvolution of the raw-clay DTG curve, accounting for overlapping kaolinite and alunite contributions, yielded an estimated kaolinite content of approximately 40.4 wt.%. Mortars incorporating clays from both calcination routes were prepared using a fixed LC^3-50 composition and tested for flexural and compressive strength at 2, 7, and 28 days. A laboratory-prepared Portland cement reference containing 95 wt.% clinker and 5 wt.% gypsum was used as the OPC control.

Compared with the raw clay, clays treated by both calcination routes exhibited reduced intensities of characteristic kaolinite reflections in their XRD patterns and less pronounced residual dehydroxylation signals in their DTG curves. All mortars containing calcined clay exhibited lower mean compressive strengths than the OPC control at 2 days, while selected mixtures reached or exceeded the control mean at 7 and 28 days. At 28 days, mean compressive strengths ranged from 29.30 to 39.15 MPa for furnace-calcined clay mixtures and from 36.13 to 40.55 MPa for solar-calcined clay mixtures, compared with 37.30 MPa for the OPC control. These findings support the technical feasibility of using solar-calcined clay in LC³-50 mortars, with selected mixtures attaining 28-day mean compressive strengths at or above the laboratory-prepared OPC reference under the investigated conditions.

Keywords: Solar Calcination, Limestone Calcined Clay Cement (LC³), Kaolinite – Alunite Clay, Thermal Activation, Low – Carbon Cement

ÖZ

GÜNEŞ DESTEKLİ KİREÇTAŞI KALSİNE KİL ÇİMENTOSU ÜRETİMİ

Yörük, Kağan Berkay
Yüksek Lisans, İnşaat Mühendisliği
Tez Yöneticisi: Doç. Dr. Çağla Meral Akgül

Eylül 2026, 85 sayfa

Çimento endüstrisi, Portland çimentosu klinkerinin enerji ve karbon yoğun üretimi nedeniyle küresel karbondioksit (CO_2) emisyonlarına önemli ölçüde katkıda bulunmaktadır. Kireçtaşı kalsine kil çimentosu (LC^3), klinkerin bir bölümünün kalsine kil ve kireçtaşı ile ikame edilmesiyle daha düşük karbonlu bir alternatif sunmaktadır. Bu çalışmada, geleneksel fırında kalsine edilmiş kil laboratuvar referansı olarak kullanılarak, güneş enerjisiyle kalsine edilmiş kilin LC^3 üretiminde kullanımının teknik uygulanabilirliği araştırılmıştır.

Yerel bir kaynaktan temin edilen kaolinit–alunit içeren kil, döner reaktöre bağlı yüksek akılı bir güneş simülatörü ve laboratuvar tipi bir kül fırını kullanılarak 550–800 °C nominal sıcaklıklarda, 0,5 ve 2 saat bekletme süreleriyle kalsine edilmiştir. Kalsinasyon sonucunda meydana gelen mineralojik ve termal değişimler, X-ışını kırınımı (XRD), termogravimetrik analiz (TGA) ve türev termogravimetri (DTG) kullanılarak incelenmiştir. Ham kilin DTG eğrisine, kaolinit ve alunitin örtüşen katkıları dikkate alınarak uygulanan Gauss pik ayrıştırması sonucunda, kaolinit içeriği kütlece yaklaşık %40,4 olarak tahmin edilmiştir. Her iki kalsinasyon yöntemiyle elde edilen killeri içeren harçlar, sabit bir LC^3-50 bileşimiyle hazırlanmış ve 2, 7 ve 28 günlük kür sürelerinin ardından eğilme ve basınç dayanımı deneylerine tabi tutulmuştur. Laboratuvarda kütlece %95 klinker ve %5 alçıtaşı kullanılarak

hazırlanan Portland çimentosu referansı, OPC kontrol karışımının bağlayıcısı olarak kullanılmıştır.

Ham kil ile karşılaştırıldığında, her iki yöntemle kalsine edilen killerin XRD desenlerinde kaolinite özgü kırınım piklerinin şiddeti azalmış ve DTG eğrilerinde kalsinasyon sonrasında kalan dehidroksilasyon sinyalleri daha az belirgin hale gelmiştir. Kalsine kil içeren tüm harçların 2 günlük ortalama basınç dayanımları OPC kontrol karışımından düşük bulunurken, bazı karışımlar 7 ve 28 günde kontrol karışımının ortalamasına ulaşmış veya bu değeri aşmıştır. Yirmi sekizinci günde ortalama basınç dayanımları, fırında kalsine edilmiş kil içeren karışımlarda 29,30–39,15 MPa, güneş enerjisiyle kalsine edilmiş kil içeren karışımlarda ise 36,13–40,55 MPa arasında değişmiş; OPC kontrol karışımında 37,30 MPa olarak ölçülmüştür. İncelenen koşullar altında bazı karışımların 28 günlük ortalama basınç dayanımlarının laboratuvarda hazırlanan OPC referansına ulaşması veya bu değeri aşması, güneş enerjisiyle kalsine edilmiş kilin LC^3-50 harçlarında kullanımının teknik açıdan uygulanabilirliğini desteklemektedir.

Anahtar Kelimeler: Güneş Enerjisiyle Kalsinasyon, Kireçtaşı Kalsine Kil Çimentosu (LC^3), Kaolinite – Alunit İçerikli Kil, Termal Aktivasyon, Düşük Karbonlu Çimento

To my family and the one I love

ACKNOWLEDGMENTS

I would like to express my sincere gratitude to my supervisor, Assoc. Prof. Dr. Çağla Meral Akgül, for her guidance, constructive feedback, and support throughout this research. Her knowledge and thoughtful suggestions helped me develop this thesis and grow as a researcher.

I also thank the members of my thesis examination committee for their careful evaluation and valuable comments, which helped improve the clarity and quality of this work.

My sincere thanks go to my friends and colleagues who helped me in the laboratory. Their practical assistance, willingness to share their experience, and companionship made the experimental work more manageable and enjoyable. I am grateful for the time and effort they generously contributed.

I owe a special debt of gratitude to my family for their unconditional love, patience, and continuous support throughout my education. I would especially like to thank my sister for her guidance and encouragement, and for generously dedicating her spare time to helping me despite her own busy schedule. Her support and encouragement made the demanding stages of this thesis easier for me.

Finally, I would like to thank my girlfriend for her love, patience, and unwavering support throughout this journey. Her understanding and encouragement helped me through challenging moments and made this experience more meaningful.

TABLE OF CONTENTS

ABSTRACT v

ÖZ vii

ACKNOWLEDGMENTS x

TABLE OF CONTENTS xi

LIST OF TABLES xiv

LIST OF FIGURES xv

CHAPTERS

1 INTRODUCTION 1

1.1 General 1

1.2 Objective and Scope 2

2 LITERATURE REVIEW 3

2.1 General 3

2.2 Limestone Calcined Clay Cement (LC^3) 4

2.2.1 Components of LC^3 8

2.2.2 Clay Calcination Methods 16

2.2.3 Hydration Mechanism of Limestone Calcined Clay Cement 21

3 EXPERIMENTAL STUDIES 23

3.1 Experimental Program 23

3.2 Raw Materials 24

3.2.1 Sources and Description of the Binder Constituents 24

3.2.2 Chemical Composition 25

3.2.3 Particle Size Distribution 27

3.2.4 Aggregate and Chemical Admixture 28

3.3 Calcination Procedure 29
3.3.1 Solar Calcination 30
3.3.2 Furnace Calcination 32
3.4 X-Ray Diffraction Analysis 37
3.5 Thermogravimetric Analysis 38
3.6 Mixture Proportions of OPC and LC³ Mortars 42
3.7 Mortar Preparation and Testing 43
3.7.1 Fresh Mortar Consistency 44
3.7.2 Specimen Preparation and Curing 46
3.7.3 Mechanical Testing 46
4 RESULTS AND DISCUSSION 47
4.1 Characterization of Raw and Calcined Clays 47
4.1.1 Mineralogical Analysis by X-Ray Diffraction 47
4.1.2 Thermal Analysis by TGA/DTG 51
4.2 Flexural Strength 56
4.3 Compressive Strength 59
4.3.1 Compressive Strength at 2 Days 60
4.3.2 Compressive Strength at 7 Days 63
4.3.3 Compressive Strength at 28 Days 65
4.4 Combined Evaluation of XRD, TGA/DTG and Compressive Strength 67
5 CONCLUSION AND RECOMMENDATIONS 69
5.1 Summary and Conclusion 69
5.2 Recommendations 71
REFERENCES 73

A. Appendix Supplementary Data on Raw Material Characterization 79

B. Appendix Temperature Profiles During Solar Calcination 80

C. Appendix Temperature Profiles During Furnace Calcination..... 83

LIST OF TABLES

Table 3.1 Oxide composition of the raw materials.....26
Table 3.2 Characteristic Particle Size Distribution of Raw Materials (μm).....28
Table 3.3 DTG Analysis with Gauss Model 41
Table 3.4 Mixture (Proportions) of OPC, LC³ and Raw-Clay Reference Mortars .43
Table 4.1 Flexural Strength values for both SLC³ and FLC³ and reference mixtures at 2, 7 and 28 days 58
Table 4.2 Compressive Strength values for both SLC³ and FLC³ and reference mixtures at 2, 7 and 28 days 59

LIST OF FIGURES

Figure 2.1 Reserve of common mineral admixtures in 2013 3
Figure 2.2 Strength gain profiles of LC³-50 systems over time, with dashed horizontal lines denoting reference Portland cement values at 3, 7, and 28 days..... 7
Figure 2.3 Chemical formulas and structural configurations of (a) kaolinite, (b) illite, and (c) montmorillonite 12
Figure 2.4 High-flux solar simulator and rotary reactor arrangement used for solar-assisted kaolin calcination..... 20
Figure 3.1 Zafer Mine in Balıkesir..... 26
Figure 3.2 Particle Size Distribution of Raw Materials (PSD) 28
Figure 3.3 Particle Size Distribution of the Aggregate Blend Compared with the Fine Aggregate Grading Limits Specified in ASTM C33/C33M 29
Figure 3.4 (a) Schematic diagram of the solar reactor and (b) construction of the tubular reactor with thermocouples (TC)..... 31
Figure 3.5 Temperature and thermal power profiles during solar calcination at a nominal target temperature of 600 °C with a holding period of 0.5 h. 32
Figure 3.6 Schematic Diagram of the Furnace Setup 33
Figure 3.7 Laboratory Furnace and Temperature - Monitoring Setup Used for Clay Calciation at Middle East Techinal University 34
Figure 3.8 Temperature Profile Recorded During Furnace Calcination at 800°C for 2 hours..... 34
Figure 3.9 Color change of calcined clays 36
Figure 3.10 XRD Patterns of the Raw Materials (Q: Quartz COD 96-901-2601, K: Kaolinite COD 96-900-9231, A: Alunite COD 96-900-0035) 37
Figure 3.11. TGA/DTG curves of raw clay 39
Figure 3.12 Deconvolution analysis on raw clay 41
Figure 3.13 The flow characteristics of the LC³ with and without superplasticizer for 600 °C - 0.5h duration. 45

Figure 4.1 XRD patterns of the raw clay and furnace-calcined clays produced at different temperatures for a) 0.5 h and b) 2 h holding periods. K: kaolinite, A: alunite, and Q: quartz 48
Figure 4.2 XRD patterns of the raw clay and the clays calcined using solar Energy produced at different temperatures for a) 0.5 h and (b) 2 h holding periods. K: kaolinite, A: alunite, and Q: quartz 50
Figure 4.3 TGA Curves of raw and solar-calcined clays 52
Figure 4.4 TGA Curves of raw and furnace-calcined clays 52
Figure 4.5 DTG curves of solar-calcined clays at different calcination temperatures for (a) 0.5 h and (b) 2 h. (Curves vertically offset for clarity) 54
Figure 4.6 DTG curves of furnace-calcined clays at different calcination temperatures for (a) 0.5 h and (b) 2 h. (Curves vertically offset for clarity) 55
Figure 4.7 Compressive Strength at 2 days of LC³ Mortars Incorporating Furnace- and Solar-Calcined Clays at Holding Times of (a) 0.5 h and (b) 2 h. 62
Figure 4.8 Compressive Strength at 7 days of LC³ Mortars Incorporating Furnace- and Solar-Calcined Clays at Holding Times of (a) 0.5 h and (b) 2 h. 64
Figure 4.9 Compressive Strength at 28 days of LC³ Mortars Incorporating Furnace- and Solar-Calcined Clays at Holding Times of (a) 0.5 h and (b) 2 h. 66

CHAPTER 1

INTRODUCTION

1.1 General

Portland cement clinker production involves substantial energy consumption and carbon dioxide (CO_2) emissions, motivating the development of binders with reduced clinker contents [1]. Supplementary cementitious materials provide opportunities for clinker substitution, although their suitability depends on their availability, composition, processing requirements, and contribution to binder performance [2].

Limestone calcined clay cement (LC^3) combines Portland clinker, calcined clay, limestone, and a calcium sulfate source to achieve substantial clinker replacement [1]. The reaction between metakaolin and limestone contributes to carboaluminate formation and pore refinement, supporting the mechanical performance of the resulting binder [3]. However, the strength development of LC^3 depends on the characteristics of the clay, including its calcined kaolinite content [4]. Thermal activation of clays are therefore an important processing step, and its effectiveness depends on the clay mineralogy and the operating conditions of the calcination system [5]. The energy required for this treatment also makes the choice of heat source relevant to the environmental performance of calcined-clay production [5].

Concentrated solar thermal energy has been investigated as an alternative heat source for processing mineral particles in directly irradiated reactors [6]. High-flux solar simulators provide controlled irradiation for experimental investigations of high-temperature thermal and thermochemical processes [7, 8]. Pasabeyoglu et al. demonstrated the calcination of kaolin using a high-flux solar simulator and a batch-operated rotary reactor, with the resulting material subsequently evaluated for zeolite

production [9] . That application provides a basis for investigating solar-assisted clay activation for other uses, including LC³. For this purpose, the mineralogical and thermal characteristics of the activated clay need to be considered together with the mechanical performance of the resulting mortars.

1.2 Objective and Scope

The primary objective of this thesis is to investigate the technical feasibility of using solar-calcined kaolinite–alunite clay as a constituent of limestone calcined clay cement (LC³). To address this objective, solar calcination was compared with conventional furnace calcination at the same nominal temperatures and holding times. This comparison examined the mineralogical and thermal changes in the treated clays and the strength development of LC³ mortars incorporating these materials, with furnace-calcined clay serving as the laboratory reference.The study addresses the following specific objectives:

1. To characterize the chemical, mineralogical, and physical properties of the constituent materials and estimate the kaolinite content of the raw clay using thermal analysis.
2. To examine the mineralogical and thermal changes in the clay following solar and furnace calcination at different nominal temperatures and holding times.
3. To evaluate the compressive and flexural strength development of LC³ mortars containing the calcined clays, using Portland cement and raw-clay-containing mortars as reference mixtures.

The experimental program covered nominal calcination temperatures of 550, 600, 650, 700, 750, and 800 °C and holding times of 0.5 and 2 h for each calcination route. Material characterization included X-ray fluorescence (XRF), X-ray diffraction (XRD), particle size distribution (PSD), and thermogravimetric and derivative thermogravimetric analysis (TGA/DTG), as applicable. Mortar strength was evaluated at 2, 7, and 28 days.

CHAPTER 2

LITERATURE REVIEW

2.1 General

Supplementary cementitious materials (SCMs) are used in blended cements to reduce clinker consumption and modify binder performance. Their contribution depends on their chemical and mineralogical composition, physical characteristics, and reactivity within the cementitious system [2]. Conventional SCMs include fly ash, ground-granulated blast-furnace slag, and silica fume, whose availability is linked to the location and production capacity of their respective industries [2]. Figure 2.1 illustrates the relative quantities of common mineral additions and cement production reported for 2013 [1].

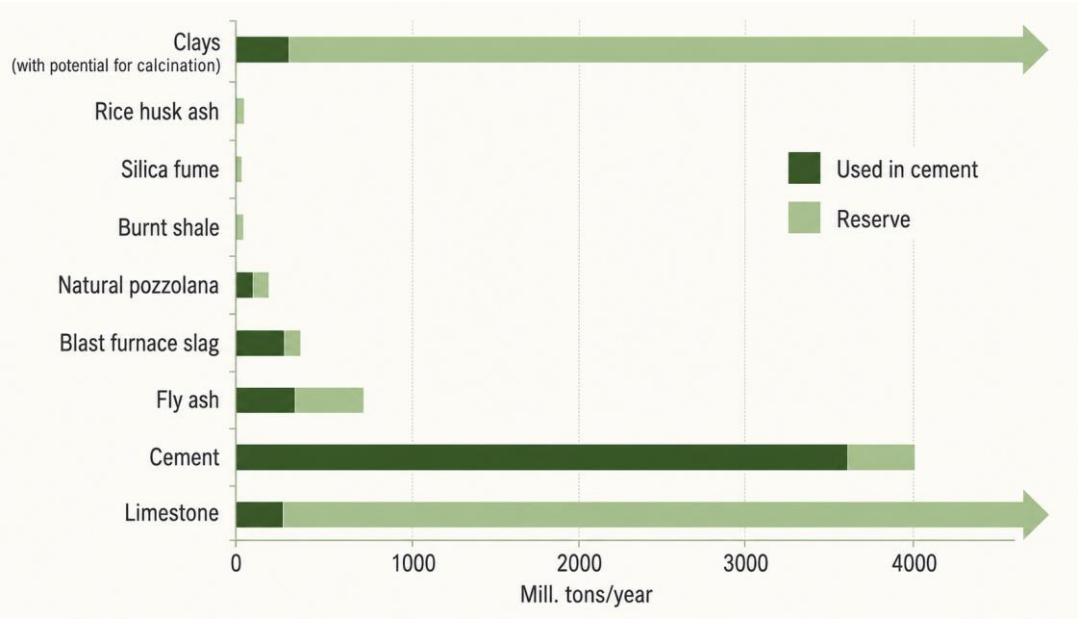

Figure 2.1 Reserve of common mineral admixtures in 2013 (adapted from [1])

Changes in industrial production and energy systems may affect the future supply of conventional SCMs, increasing interest in alternative sources [2]. Calcined clays are particularly relevant because clay resources are widely distributed and suitable clay minerals can develop pozzolanic reactivity through thermal activation [1, 5]. However, the response to calcination differs among clay minerals, making mineralogical composition an important factor in precursor selection and processing [10].

The combined use of calcined clay and limestone provides an additional opportunity for clinker substitution. Antoni et al. showed that their combined incorporation could maintain or improve mortar strength relative to a Portland cement reference under the conditions investigated [11]. Subsequent research demonstrated that the interaction between metakaolin and limestone contributes to carboaluminate formation and pore refinement [3]. These findings provide the basis for LC³, whose performance depends on the properties and proportions of its constituents [1].

The properties of LC³ depend on the characteristics and proportions of its constituents, the mineralogical composition and thermal activation of the clay, and the reactions occurring during hydration [1, 5, 12]. In addition, the environmental performance of LC³ can be further improved by reducing the fossil-fuel-derived energy required for clay calcination [13, 14].

The following sections review the principal characteristics of LC³, its constituent materials, the production and activation of calcined clay through conventional and solar-aided processes, and the hydration mechanisms governing the development of the resulting cementitious system.

2.2 Limestone Calcined Clay Cement (LC³)

Limestone calcined clay cement (LC³) is a blended cement system comprising Portland clinker, calcined clay, limestone, and a calcium sulfate source, commonly gypsum [1]. Although limestone and calcined clay have individually been

incorporated into cementitious materials for many years, their combined use enables greater clinker replacement by taking advantage of their complementary physical and chemical contributions [1, 11]. The development of LC³ therefore extends beyond the partial substitution of clinker with a single supplementary material and involves the selection of constituents that interact beneficially during hydration [11]. LC³-based binders have been associated with reductions of approximately 40% in embodied CO_2 compared with ordinary Portland cement [1]. This reduction should be understood in relation to the composition and production conditions of the systems being compared, since the environmental benefit depends on factors such as clinker content, clay processing, and the energy required for calcination [1, 5].

The most widely investigated formulation is LC³-50, in which the number denotes a clinker content of approximately 50% by mass [1]. A typical composition consists of 50% clinker, 30% calcined clay, 15% limestone, and 5% gypsum, corresponding to a calcined-clay-to-limestone mass ratio of 2:1 [1, 15]. This formulation provides a practical reference for studying the combined contribution of the two supplementary constituents while maintaining a substantially reduced clinker content [11]. Nevertheless, these proportions should not be regarded as universally optimal, because the behavior of the binder depends on the mineralogical composition and reactivity of the clay, the fineness of the constituents, and the sulfate balance of the system [11, 16, 17]. Consequently, the use of an established LC³-50 composition does not eliminate the need to characterize the constituent materials and evaluate the performance of the resulting mixture.

The mechanical performance of LC³ cannot be explained solely by clinker dilution. Calcined clay supplies reactive aluminosilicate phases that participate in pozzolanic reactions, whereas finely ground limestone contributes through physical effects and chemical interactions with the reactive alumina available in the binder [4, 11]. The interaction between metakaolin and limestone promotes the formation of hemicarboaluminate and monocarboaluminate hydrates, whose precipitation contributes to pore refinement and strength development [1]. These reactions provide a chemical basis for combining calcined clay and limestone rather than treating both

constituents as equivalent inert replacements [11]. Antoni et al. reported that the combined replacement of Portland cement with 30% metakaolin and 15% limestone produced higher compressive strengths at 7 and 28 days than the Portland cement reference under their experimental conditions [11]. This finding provided an important foundation for the development of LC³ by demonstrating that substantial substitution could be accompanied by satisfactory, and in that study improved, mechanical performance.

The suitability of a clay for LC³ production is closely related to its mineralogical composition and the reactivity developed during calcination [5, 10]. Kaolinitic clays have received particular attention because the dehydroxylation of kaolinite produces metakaolin, a disordered aluminosilicate phase with substantial pozzolanic potential [10]. Calcination temperatures commonly fall within approximately 600–850 °C for kaolinitic materials, although the appropriate treatment depends on the properties of the clay and the operating conditions of the calcination system [5, 15]. Temperature must therefore be considered together with residence time and heat-transfer conditions when assessing the suitability of a calcined clay [5].

High-purity kaolin is not essential for LC³ production, which broadens the range of potentially suitable raw materials [1]. Lower-grade kaolinitic clays may contain substantial quantities of associated minerals and may be unsuitable for applications that require high purity or a particular color, while still providing a useful source of reactive material after calcination [15]. Krishnan et al. discussed the suitability of clays containing kaolinite contents as low as approximately 40%, including materials containing iron-bearing impurities that limit their attractiveness to the ceramic industry [15]. The possibility of utilizing such resources is an important practical advantage of LC³, particularly where conventional supplementary cementitious materials are unavailable or limited in supply [1]. However, the kaolinite content should be interpreted together with the nature of the accompanying minerals and the effectiveness of thermal activation, rather than used as an independent guarantee of performance [5, 10].

Avet and Scrivener investigated the influence of calcined kaolinite content using seven kaolinitic clays of different origins and compositions, with initial kaolinite contents ranging from approximately 17% to 95% [4]. The clays were evaluated in an LC³-50 formulation containing 50% clinker, 30% calcined clay, 15% limestone, and 5% gypsum [4]. Their investigation demonstrated that calcined kaolinite content strongly influenced hydration and strength development, particularly at early ages [4]. At later ages, the differences between mixtures containing intermediate and high calcined kaolinite contents became less pronounced, indicating that increasing clay purity did not produce a proportional improvement in strength throughout the hydration period [4]. The strength-development profiles presented in Figure 2.2 illustrate this relationship and the performance of the investigated mixtures relative to the Portland cement reference [4]. These findings support the use of appropriately selected lower-grade clays and emphasize the importance of evaluating clay quality in the context of the complete LC³ binder.

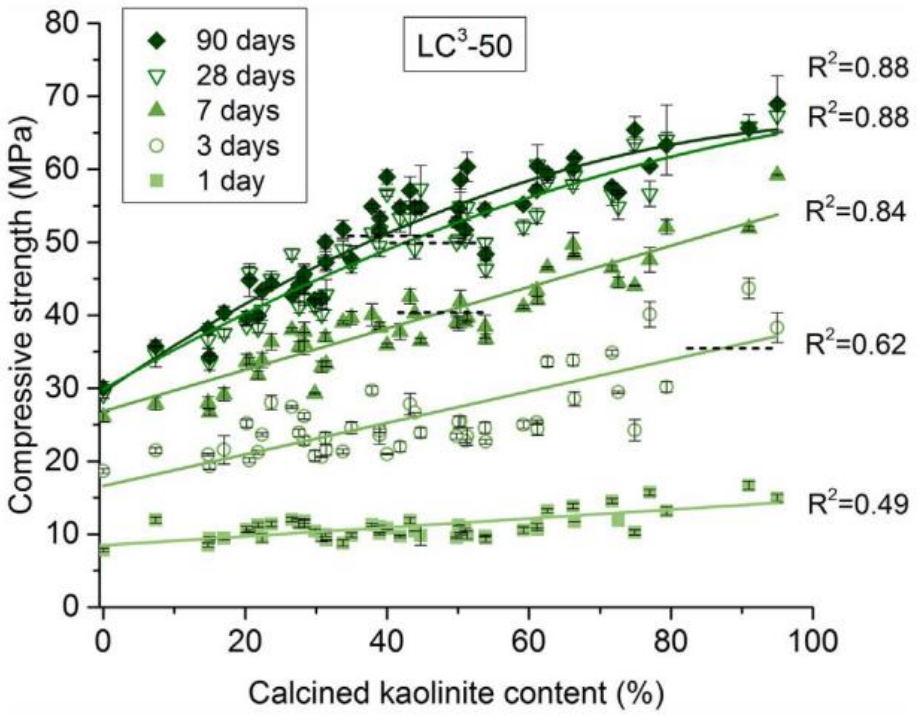

Figure 2.2 Strength gain profiles of LC³-50 systems over time, with dashed horizontal lines denoting reference Portland cement values at 3, 7, and 28 days [4].

The feasibility of LC³ production has also been investigated beyond laboratory-scale mixture development. Krishnan et al. reported industrial trial production at three locations in India, using locally available raw materials and different combinations of calcination and grinding equipment [15]. Both static and rotary calciners were employed, together with open- and closed-circuit ball mills, demonstrating that LC³ production could be investigated using more than one processing arrangement [15]. The trials also included limestones of different compositions and showed that lower-grade clay and limestone could be utilized, with production quality assessed using widely available characterization techniques [15].

Practical applications further demonstrated the potential use of the resulting cement in construction. These included an LC³ demonstration house at Orchha, near Jhansi, where LC³ was used in structural and non-structural elements, and autoclaved aerated concrete blocks used for the walls of a building within the Swiss Embassy complex in New Delhi [15]. These examples extend the evidence for LC³ from laboratory strength measurements to the production and application of building components [15]. Nevertheless, the range of materials and equipment employed in these trials also highlights the need for appropriate raw-material selection and process control to obtain consistent binder performance [15]. The following section therefore examines the individual constituents of LC³ and their contributions to the behavior of the combined system.

2.2.1 Components of LC³

The performance of LC³ depends on the combined contributions of Portland cement clinker, calcined clay, limestone, and a calcium sulfate source [1]. These constituents influence the supply of reactive species, the progress of hydration, and the physical characteristics of the binder [11, 17]. Their functions are interdependent: clinker hydration provides products that participate in the reaction of calcined clay, while limestone and calcium sulfate influence the formation of aluminate-bearing hydrates

[1, 11]. Therefore, understanding the role of each constituent is necessary for evaluating how variations in raw-material properties affect LC³ performance.

2.2.1.1 Portland cement clinker

Portland cement clinker supplies the principal hydraulic phases of LC³, including alite, belite, tricalcium aluminate, and ferrite [1]. The hydration of the calcium silicate phases produces calcium silicate hydrate (C–S–H), which provides the principal binding contribution, and calcium hydroxide, commonly referred to as portlandite [1]. Portlandite subsequently participates in the pozzolanic reaction of the activated aluminosilicate phases supplied by calcined clay [11]. Clinker therefore contributes both directly to hydrate formation and indirectly to the reaction of the supplementary constituents.

The chemical and mineralogical composition of clinker also influences the behavior of the aluminate-bearing phases. Differences in clinker aluminate content affect the availability of aluminium for reactions involving sulfate and carbonate, while alkali contents influence the chemical environment in which hydration proceeds [17, 18]. Consequently, clinkers with different compositions may produce different hydration responses even when the calcined-clay and limestone replacement levels are unchanged [17]. Clinker composition must therefore be considered alongside the properties of the supplementary constituents when selecting mixture proportions and evaluating the sulfate balance of LC³.

2.2.1.2 Limestone

Limestone is incorporated into LC³ primarily as finely ground calcium carbonate [9]. Its contribution involves both physical effects and chemical participation in hydration. Fine limestone particles can provide additional surfaces for hydrate precipitation and influence particle packing, with these effects depending on their fineness relative to the other constituents [11, 16]. Limestone fineness is therefore

relevant to the behavior of the mixture, rather than being solely a processing characteristic.

Limestone also reacts with aluminium-bearing species released during the hydration of clinker and the reaction of calcined clay, promoting the formation of hemicarboaluminate and monocarboaluminate hydrates [11, 18]. Zunino and Scrivener showed that the reaction between metakaolin and limestone contributes to pore refinement and mechanical development through the formation of additional hydration products [3]. This chemical contribution explains why limestone behaves differently from an inert filler in a binder containing sufficient reactive alumina [3]. Its effectiveness nevertheless depends on the availability of the other reactants, so increasing limestone content alone does not necessarily produce a corresponding increase in hydrate formation or strength [11].

The composition of the limestone source should also be considered. Industrial LC^3 trials have investigated limestones with different impurity contents and alternative carbonate-bearing materials, demonstrating that the suitability of a source cannot be assessed solely by applying the requirements used for clinker manufacture [15]. Variations in carbonate content and associated minerals can affect the amount of material available for chemical reaction and the physical characteristics of the binder [15]. Accordingly, limestone purity and fineness should be reported when comparing LC^3 mixtures prepared using different raw materials.

Unlike the limestone used as a raw material for clinker production, the limestone added during LC^3 blending is generally incorporated without calcination [1]. Its use therefore contributes to clinker substitution without requiring the carbonate decomposition associated with clinker manufacture [1]. This processing distinction forms part of the environmental rationale for combining limestone with calcined clay.

2.2.1.3 Gypsum

Gypsum is incorporated into LC^3 as a calcium sulfate source to regulate the hydration of aluminate-bearing clinker phases [1]. Its dissolution supplies sulfate for the formation of ettringite and helps control the early aluminate reactions [18]. Gypsum therefore contributes to the development of the hydrate assemblage and the coordination of the reactions occurring during the initial stages of hydration [11].

The appropriate gypsum content depends on the characteristics of the complete binder, including clinker composition, calcined-clay reactivity, and constituent fineness [17]. Insufficient sulfate availability may lead to premature sulfate depletion and alter the timing of aluminate reactions, whereas excessive gypsum addition may leave residual calcium sulfate or modify the subsequent hydration behavior [11, 17]. Consequently, the gypsum content adopted in a reference LC^3 formulation should not automatically be regarded as optimal for every combination of constituent materials [17].

In the present study, the gypsum content was adopted from the widely used LC^3-50 formulation, comprising 50% clinker, 30% calcined clay, 15% limestone, and 5% gypsum by mass [1, 15]. This composition was selected on the basis of its established use in laboratory investigations and industrial trials, which have demonstrated the feasibility of substantial clinker replacement while maintaining satisfactory mechanical performance [4, 15]. Accordingly, the gypsum proportion was retained at 5% in accordance with this formulation.

2.2.1.4 Calcined Clay

Clay is a naturally occurring, fine-grained material that generally develops plasticity when mixed with an appropriate amount of water and becomes harder after drying or firing [19]. It forms through the weathering and alteration of rocks and may contain several clay minerals together with associated constituents such as quartz, feldspars, carbonates, and iron-bearing minerals [20]. Although particle size is an

important characteristic, clay cannot be defined solely by a universal size threshold because the adopted classifications differ among scientific disciplines [19]. Its suitability for cementitious applications consequently requires consideration of mineralogical composition as well as physical characteristics [2, 10].

Clay minerals are hydrous phyllosilicates whose structures consist of tetrahedral and octahedral sheets arranged in different configurations [20, 21]. Kaolinite has a 1:1 structure comprising one silica tetrahedral sheet linked to one alumina octahedral sheet, whereas illite and montmorillonite have 2:1 structures in which an octahedral sheet is located between two tetrahedral sheets [20–22]. These differences in sheet arrangement and interlayer bonding influence water adsorption, swelling behavior, ion-exchange capacity, and the response to thermal treatment [20, 21]. The representative structures and chemical compositions of these minerals are presented in Figure 2.3.

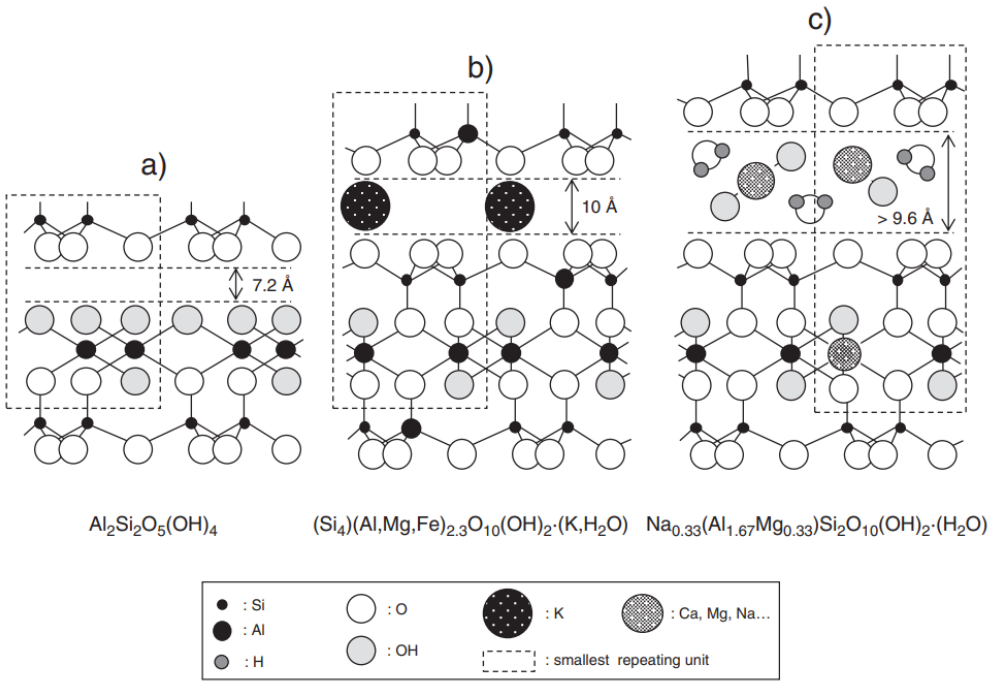

Figure 2.3 Chemical formulas and structural configurations of (a) kaolinite, (b) illite, and (c) montmorillonite [10].

Raw clay minerals generally exhibit limited pozzolanic reactivity because much of their silica and alumina remains within ordered crystalline structures [10]. Thermal activation, commonly referred to as calcination, is applied to modify these structures and produce phases that can react in cementitious environments [5]. The reactivity developed through this treatment depends on the original mineralogy and on processing conditions, including temperature, residence time, heating rate, particle size, and heat transfer within the calciner [5]. Calcined clay should therefore be understood as a material whose properties reflect both its geological origin and its thermal processing history.

Kaolinite, with the ideal chemical formula $Al_2Si_2O_5(OH)_4$, is particularly relevant because its thermal activation produces the disordered aluminosilicate material commonly known as metakaolin [10]. The transformation involves the removal of structural hydroxyl groups through dehydroxylation and can be represented by the following simplified reaction [5, 10]:

$$Al_2Si_2O_5(OH)_4 \rightarrow Al_2Si_2O_7 + 2H_2O \quad (2.1)$$

The initial stages of heating involve the removal of physically adsorbed water and, depending on the minerals present, interlayer water [5]. These processes should be distinguished from dehydroxylation, which involves hydroxyl groups within the mineral structure [5]. Kaolinite dehydroxylation commonly occurs over approximately 400–700 °C, although the position and breadth of the thermal event depend on crystallinity, particle characteristics, and experimental heating conditions [5, 23]. Calcination temperatures of approximately 600–850 °C are frequently employed for kaolinitic clays, with the selected temperature and residence time intended to provide sufficient activation [12].

Dehydroxylation and the development of structural disorder are closely related, but they should not be treated as interchangeable measures of pozzolanic reactivity [5, 10]. The disappearance of characteristic kaolinite reflections indicates a loss of detectable crystalline order, while the reduction of residual dehydroxylation in thermal analysis provides complementary information about the progress of thermal

transformation. These observations are useful for assessing activation, but the performance of the calcined product also depends on its resulting structure and its ability to react within the binder [10, 24].

The selection of calcination conditions requires a balance between incomplete activation and excessive thermal treatment [5]. Insufficient temperature or residence time may leave residual kaolinite in the product and limit the amount of activated material [5]. Conversely, excessive treatment can promote structural reorganization, particle sintering, and the formation of phases with lower reactivity [5, 24]. Alujas et al. demonstrated the importance of calcination temperature and the resulting phase assemblage when evaluating the pozzolanic reactivity of low-grade kaolinitic clays [24]. Accordingly, the temperature required for effective activation should be considered in relation to the particular clay and the processing conditions rather than expressed as a single universal value.

Different clay minerals also respond differently to thermal treatment. Fernández et al. compared kaolinite, illite, and montmorillonite and related their different pozzolanic activities to the structural changes produced during calcination [10]. Kaolinite generally develops greater reactivity because its activation produces substantial structural disorder, whereas thermally treated illite and montmorillonite may retain a greater degree of structural organization [10]. Nevertheless, these minerals can also contribute to cementitious reactions, and their performance depends on mineral composition and activation conditions [10, 16]. This distinction is relevant when evaluating natural clays, which commonly contain mixtures of minerals rather than a single pure phase.

High-purity kaolin is not essential for LC^3 production, and lower-grade kaolinitic clays provide an opportunity to use resources that may be unsuitable for more demanding industrial applications [1, 15]. However, the associated minerals must be considered when interpreting the behavior of the calcined product. Quartz and feldspars generally make a limited direct contribution to the pozzolanic reaction under conventional clay activation conditions, while other constituents may undergo

their own thermal transformations [5]. The presence of carbonate minerals within the raw clay also requires attention because their behavior during calcination differs from that of limestone incorporated separately during binder preparation [24]. Consequently, total chemical composition alone is insufficient to describe the amount and nature of the reactive material developed during activation [2, 10].

2.2.1.4.1 Alunite in Kaolinitc Clays

Alunite requires particular consideration in the clay investigated in this thesis. It is a hydroxyl- and sulfate-bearing mineral with the ideal formula $KAl_3(SO_4)_2(OH)_6$ and is mineralogically distinct from kaolinite [25, 26]. Its presence introduces thermal events that must be distinguished from the dehydroxylation of kaolinite when interpreting the behavior of a mixed clay. Mohammadi and Salarirad investigated alunite dehydroxylation and showed that its progress depends on temperature and treatment time [25]. Küçük and Yıldız reported a principal thermal event near 560 °C associated with dehydroxylation and a higher-temperature event near 820 °C associated with desulfation for the non-mechanically activated material investigated in their study [26]. These values describe particular experimental materials and conditions and should not be applied as fixed peak positions for every alunite-bearing clay.

The thermal behavior of pure or relatively pure minerals provides a useful basis for interpreting natural clay mixtures, but overlapping events can complicate individual phase assignments [25–27]. This is particularly relevant where kaolinite and alunite coexist, because a measured mass loss may contain contributions from more than one transformation. The identification of a DTG peak should therefore be evaluated alongside the mineral phases detected by XRD and the thermal behavior reported for the relevant minerals. In this thesis, alunite is considered in relation to raw-clay mineralogy and thermal characterization.

The geological setting of the investigated clay provides further context for this mineral association. Ece et al. described the Düvertepe deposits, located at the western end of the Simav Graben in Türkiye, as hydrothermal kaolin deposits formed through the alteration of Miocene rhyolitic–rhyodacitic volcanic rocks and tuffs [28]. Hydrothermal fluids circulated through fault and fracture systems, promoting alteration of the volcanic materials [28]. The deposits include a kaolinite-dominated assemblage containing kaolinite, alunite, and quartz, and an alunite-dominated assemblage containing alunite, opal-CT, quartz, and halloysite [28]. This geological description explains the regional coexistence of kaolinite, alunite, and silica-bearing phases, but does not establish their proportions in the particular sample investigated here. The composition of that sample must be determined from its own characterization results.

2.2.2 Clay Calcination Methods

Clay calcination can be performed using static furnaces, rotary kilns, flash calciners, and other reactor configurations that provide the thermal conditions required for activation [5]. Although these systems serve the same general purpose, they differ in heating mechanism, material movement, residence time, and the distribution of temperature within the processed material [5]. Consequently, a specified calcination temperature does not fully describe the treatment experienced by the clay. The operating conditions must also be considered when interpreting the properties of the calcined product and comparing results obtained using different systems [5].

Static or muffle furnaces are commonly used for laboratory investigations because they allow convenient control of furnace temperature and holding time [5]. In these systems, the clay is generally placed in a crucible or tray and remains stationary during heating. Heat is transferred from the furnace environment to the container and the exposed material, followed by heat transfer through the clay bed [5]. The temperature measured by the furnace control sensor may therefore differ from the temperature within the sample, particularly during heating or when relatively large

batches and thick material beds are used [5]. The nominal furnace temperature and the duration for which it is maintained should consequently be reported together with sample preparation, batch size, and temperature-measurement conditions.

Rotary kilns provide a different thermal environment by introducing material movement during heating [12]. Rotation causes the particles to move within the reactor, changing their exposure to heated surfaces and the surrounding gas and promoting mixing within the material bed [5, 6]. The resulting heat transfer depends on reactor geometry, rotational speed, filling level, and the flow behavior of the particles [6]. These characteristics are particularly relevant for fine, cohesive materials, whose movement may differ from that of freely flowing granular solids [6]. Rotation can improve the distribution of thermal exposure, but it does not by itself establish that all particles experience an identical temperature history.

The applicability of different calcination arrangements has been demonstrated in LC³ production trials. Krishnan et al. reported the use of both static and rotary calciners during industrial investigations in India [15]. The production program also employed open- and closed-circuit ball mills, illustrating that clay activation and subsequent material preparation can be carried out through different equipment combinations [15]. These experiences demonstrate the flexibility of LC³ production, while also emphasizing that the processing conditions must be evaluated in relation to the characteristics of the available raw materials [15].

Flash calcination relies on rapid heat transfer between fine particles and a hot gas stream, with residence times typically on the order of seconds [5]. The short treatment period distinguishes this process from static and rotary systems in which the material may remain at elevated temperatures for substantially longer periods [5]. Effective operation requires control of particle size, initial moisture, gas temperature, and gas–solid contact to obtain sufficient activation within the available residence time [5]. A short residence time does not necessarily indicate insufficient treatment, because the rate of heat transfer and the temperature reached by individual particles can differ considerably from those in a stationary clay bed. Conversely, the gas

temperature cannot be interpreted directly as the particle temperature without considering the heat-transfer conditions [5].

Holding time and residence time should therefore be defined according to the operating mode of the calcination system. In batch experiments, a reported holding time describes a period maintained after a selected temperature criterion has been reached, making the location and role of the temperature sensor important to its interpretation. In continuous systems, residence time describes the duration of material passage through the reactor, during which the temperature may change along the processing path [5]. Even for two batch systems, equal holding times do not establish equivalent treatments if the heating ramps, sample temperatures, material movement, or cooling conditions differ. These distinctions are important when comparing laboratory furnace treatment with a batch-operated solar reactor.

Concentrated solar thermal energy provides an alternative means of supplying heat for mineral processing. In directly irradiated systems, concentrated radiation enters the reactor and is absorbed by the material and the internal reactor surfaces [6]. The distribution of absorbed energy depends on the optical arrangement, reactor geometry, exposed surfaces, and movement of the particles [6]. Moumin et al. investigated the solar treatment of cohesive particles in a directly irradiated rotary kiln, demonstrating the relevance of particle behavior and reactor operation to the thermal processing of such material [6]. Solar calcination must therefore be evaluated as a coupled irradiation and heat-transfer process, rather than solely in terms of a target reactor temperature.

High-flux solar simulators are used to investigate these processes under controlled laboratory conditions. Xenon short-arc lamps and concentrating optical components can produce intense irradiation suitable for high-temperature thermal and thermochemical research [7, 8]. Such facilities allow experiments to be performed independently of changes in natural solar availability and provide greater control over the applied irradiation [7, 8]. Dibowski et al. described a high-flux simulator at DLR comprising ten xenon short-arc lamps and elliptical reflectors, designed to

concentrate approximately 20 kW of radiative power onto a focal region of approximately 100 cm² [29]. These specifications characterize the facility and should be distinguished from the power actually supplied to a reactor during a particular experiment.

A solar simulator reproduces an irradiation environment for research purposes; the lamps themselves are electrically powered [7, 8]. Accordingly, experiments conducted with a simulator establish the technical response of the reactor and material under the applied irradiation conditions. They do not directly measure the environmental performance of an installation operating with natural concentrated sunlight. The potential environmental benefit of solar-assisted clay activation must instead be evaluated by considering the energy source, system boundaries, and operating conditions of the proposed application.

Pasabeyoglu et al. demonstrated solar-assisted kaolin calcination using a high-flux solar simulator and a batch-operated rotary reactor [9]. Concentrated radiation entered the reactor through an aperture, while rotation promoted movement of the kaolin bed within the cavity [9]. Approximately 1 kg of kaolin was treated at measured bed temperatures ranging from 740 to 980 °C, with a nominal holding period of 2 h [9]. XRD and spectroscopic analyses supported the transformation of kaolinite into metakaolin over the investigated treatment conditions [9]. The study therefore provided experimental evidence that concentrated irradiation could supply the heat required for kaolin activation. The arrangement of the high-flux solar simulator and rotary reactor used in that study is shown in Figure 2.4 [9].

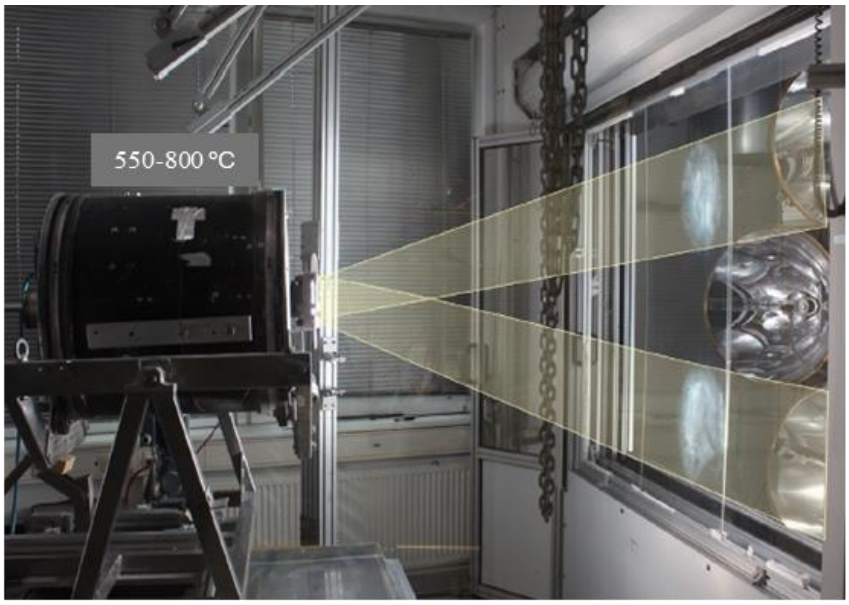

Figure 2.4 High-flux solar simulator and rotary reactor arrangement used for solar-assisted kaolin calcination [9].

An important observation in that investigation was the variation between temperatures recorded at different positions within the reactor [9]. This finding illustrates why wall, cavity, control, and material-bed temperatures should not be used interchangeably when describing a calcination experiment. The reported temperature must be associated with a clearly identified measurement location, and the interpretation of activation should consider the thermal history experienced by the material itself [9]. This distinction is especially relevant when comparing reactors with different heating mechanisms and material-motion conditions.

The calcined products investigated by Pasabeyoglu et al. were evaluated as precursors for zeolite synthesis [9]. Their successful application provides a basis for further investigation of solar-assisted clay processing, but the requirements of that application differ from the assessment of a constituent for LC^3. For cementitious use, the characteristics of the calcined clay must be considered together with its contribution to the performance of the resulting binder. The present study therefore examines mineralogical and thermal changes alongside mortar strength, while

interpreting the furnace and solar results within their respective experimental conditions.

2.2.3 Hydration Mechanism of Limestone Calcined Clay Cement

The hydration of limestone calcined clay cement is governed by the combined reactions of Portland cement clinker, calcined clay, limestone, and gypsum. Besides the typical hydration reactions of ordinary Portland cement, LC³ hydration involves the dissolution of metakaolin, its pozzolanic reaction with portlandite, and the interaction between limestone and the alumina released from clinker and calcined clay. These coupled reactions produce additional hydrates and explain the synergistic behaviour of calcined clay and limestone in LC³ [11].

Following water addition, clinker hydration creates a calcium-rich and highly alkaline pore solution. The hydroxyl ions in this solution attack the disordered aluminosilicate structure of metakaolin, promoting the release of dissolved aluminate and silicate species. This dissolution process can be represented in simplified form as:

$$Al_2O_3(SiO_2)_2 + 6\,OH^- + 3H_2O \rightarrow 2Al(OH)_4^- + 2H_2SiO_4^{2-} \qquad (2.2)$$

The dissolved species subsequently react with calcium ions and portlandite produced during clinker hydration. This pozzolanic reaction consumes portlandite and forms additional calcium–aluminosilicate hydrate (C–A–S–H) together with alumina-containing hydrates such as strätlingite. Using cement chemistry notation, the overall reaction of metakaolin may be expressed schematically as:

$$AS_2 + 3CH + 6H \rightarrow C - A - S - H + C_2ASH_8 \qquad (2.3)$$

where AS_2 represents metakaolin, CH represents portlandite, and C_2ASH_8 represents strätlingite. Equation (2.3) is a simplified representation because the composition and relative quantities of the hydration products depend on the availability of calcium, aluminium, sulfate, and water. Aluminium released from metakaolin may also be incorporated into the C–S–H structure, resulting in the formation of C–A–S–

H with a generally lower Ca/Si ratio than the C–S–H formed in ordinary Portland cement [11].

Limestone participates in LC³ hydration through both physical and chemical effects. Fine limestone particles provide additional nucleation surfaces for hydrate precipitation, while a fraction of the calcium carbonate reacts with dissolved alumina. This reaction primarily produces hemicarboaluminate and monocarboaluminate hydrates. Their formation from clinker aluminates can be represented as:

$$C_3A + C\bar{C} + 11H \rightarrow C_4A\bar{C}H_{11} \quad (2.4)$$

$$C_3A + 0.5C\bar{C} + 0.5CH + 11.5H \rightarrow C_4A\bar{C}_{0.5}H_{12} \quad (2.5)$$

Where $C\bar{C}$ represents calcium carbonate, $C_4A\bar{C}H_{11}$ is monocarboaluminate, and $C_4A\bar{C}_{0.5}H_{12}$ is hemicarboaluminate. Limestone can also react with aluminium released directly from metakaolin, demonstrating the chemical synergy between the two supplementary constituents:

$$AS_2 + 0.5C\bar{C} + 3.5CH + 8.5H \rightarrow C_4A\bar{C}_{0.5}H_{12} \quad (2.6)$$

The formation of carboaluminate phases modifies the AFt–AFm phase assemblage of the hydrated binder. Carbonate supplied by limestone favours hemicarboaluminate and monocarboaluminate formation instead of monosulfoaluminate [18] thereby contributing to the stabilisation of ettringite. The resulting increase in the volume of solid hydrates, together with additional C–A–S–H formation, refines the pore structure and supports strength development. Therefore, limestone is not merely an inert filler in LC³; it chemically interacts with the reactive alumina supplied by clinker and metakaolin [4, 11].

CHAPTER 3

EXPERIMENTAL STUDIES

3.1 Experimental Program

The experimental program comprised clay preparation and calcination, characterization of the Portland cement clinker, limestone, gypsum and raw/calcined clays and evaluation of mortar performance. The same raw clay was treated using a high-flux solar simulator and a laboratory furnace at six nominal calcination temperatures: 550, 600, 650, 700, 750, and 800 °C. Two holding periods, 0.5 and 2 h, were investigated at each temperature, resulting in twelve calcination conditions for each route.

The nominal temperature and holding-time matrix provided a common framework for comparing the two calcination routes. However, the routes differed in their heating arrangements and material movement; therefore, matching nominal conditions did not necessarily imply identical temperature histories within the clay. The temperature measurements and the criteria used to define the holding period are described under the respective calcination procedures.

The resulting calcined clays were incorporated into mortars using a fixed LC^3-50 binder composition comprising 50 wt. % clinker, 30 wt. % calcined clay, 15 wt. % limestone, and 5 wt. % gypsum. This formulation was selected as an established reference composition widely investigated in previous laboratory and industrial studies [1, 11, 15]. Maintaining the same binder proportions provided a consistent basis for examining the performance of clays produced under different calcination conditions.

A reference binder consisting of 95 wt.% Portland cement clinker and 5 wt.% gypsum was prepared and designated as OPC throughout this thesis. A second

reference mixture was prepared by replacing the calcined clay in the LC³-50 formulation with the same mass of uncalcined clay. These reference mixtures provided a basis for evaluating the effects of clinker replacement and clay calcination on mortar strength. Flexural and compressive strengths were measured after 2, 7, and 28 days of curing.

3.2 Raw Materials

The materials used in this study comprised a locally sourced clay, Portland cement clinker, limestone, gypsum, sand, and a polycarboxylate ether-based superplasticizer. The clay was subjected to solar and conventional furnace calcination before being incorporated into LC³ mortars. Uncalcined clay was also used in a reference blend to evaluate the influence of thermal treatment.

3.2.1 Sources and Description of the Binder Constituents

The clay was obtained from the Zafer Mine in Balıkesir, Türkiye. The location and an overview of the mine are presented in Figure 3.1. The material contained kaolinite together with quartz and alunite, as identified by X-ray diffraction. The same source clay was used for both calcination routes to provide a common starting material for evaluating the effects of temperature, holding time, and calcination method.

Portland cement clinker was supplied by Baştaş Cement Factory in Ankara, Türkiye. It was used as the clinker component of the LC³ binders and of the Portland cement reference binder. Limestone was obtained from Kimyacınız Kimyevi Maddeler Sanayi ve Ticaret in Istanbul, Türkiye, and was incorporated as the limestone constituent of the LC³ blends.

Gypsum was also supplied by Baştaş Cement Factory. It was included as the calcium sulfate component of the binders, with its proportion specified in the mixture design.

A fixed LC^3-50 composition was adopted throughout the calcined-clay mortar program.

3.2.2 Chemical Composition

The chemical compositions of the raw materials are presented in Table 3.1. Since the XRF results were originally normalized on an LOI-free basis, the oxide contents were recalculated by incorporating the separately determined loss-on-ignition values. Minor oxide constituents were collectively represented as "Others," and the complete analytical results are provided in Apendix A.

3.2.2.1 Chemical Composition of Raw Clay

The raw clay contained 52.45 wt. % SiO_2 and 27.81 wt. % Al_2O_3, demonstrating its predominantly aluminosilicate composition. These bulk oxide contents were considered together with the XRD results to characterize the material, since chemical composition alone does not distinguish between individual crystalline minerals. The clay also contained 2.54 wt. % Fe_2O_3, 2.54 wt. % SO_3, and 0.78 wt. % K_2O. The mineralogical identification and thermal characterization of the clay are addressed in the relevant sections.

3.2.2.2 Chemical Composition of Limestone

The limestone was predominantly composed of CaO, with a content of 54.60 wt. %, confirming its high carbonate purity. The low concentrations of SiO_2, Al_2O_3, and Fe_2O_3 indicated a negligible contribution from siliceous and clay-bearing impurities, while the minor MgO content was attributed to magnesium-bearing carbonate phases.

3.2.2.3 Chemical Composition of Gypsum

The gypsum was characterized principally by CaO and SO_3 contents of 32.71 and 39.68 wt. %, respectively. SiO_2 and Al_2O_3 were present at 2.24 and 0.77 wt. %, indicating that the supplied material also contained minor constituents in addition to its calcium sulfate component.

3.2.2.4 Chemical Composition of Portland Cement Clinker

The clinker contained 65.43 wt. % CaO and 18.25 wt. % SiO_2. Its Al_2O_3 and Fe_2O_3 contents were 4.94 and 4.92 wt. %, respectively. These values establish the bulk chemical composition of the clinker used in both the reference and blended binders.

Figure 3.1 Zafer Mine in Balıkesir

Table 3.1 Oxide composition of the raw materials

Oxides (wt%)	SiO_2	Al_2O_3	Fe_2O_3	CaO	K_2O	MgO	SO_3	LOI(*)
Clay	52.45	27.81	2.54	0.54	0.78	0.21	2.54	12.0
Limestone	0.09	0.05	0.03	54.60	0.00	1.14	0.08	44.0
Gypsum	2.24	0.77	0.50	32.71	0.13	0.37	39.68	23.4
Clinker	18.25	4.94	4.92	65.43	1.11	1.11	1.14	1.90

(*) LOI: Loss on ignition. Determined by ASTM D7348

3.2.3 Particle Size Distribution

The clinker, limestone, and gypsum were supplied in ground form and used without further grinding. Before characterization, the raw clay was dried and mechanically deagglomerated to break up lumps formed during moist storage. This treatment was intended to disperse agglomerates rather than reduce the size of the individual mineral particles. The clay preparation procedure is described in Section 3.3.

Figure 3.2 presents the particle size distributions of the raw clay, clinker, limestone, and gypsum. The corresponding characteristic particle sizes obtained from the PSD analysis are summarized in Table 3.2. D10, D50, and D90 denote the particle diameters below which 10%, 50%, and 90% of the cumulative particle volume lie, respectively, while D[4,3] represents the volume-weighted mean diameter. Among the raw materials, clinker exhibited the coarsest particle size distribution, with a D50 of 14.5 μm and D[4,3] of 18.1 μm. In comparison, limestone and gypsum showed finer distributions, with D50 values of 7.5 and 6.3 μm, respectively. The raw clay had the lowest D50 among these materials at 5.5 μm; however, its relatively high D90 value of 32.5 μm indicates a broader particle size distribution extending toward larger particle sizes. Overall, the PSD results demonstrate distinct particle size characteristics among the constituent materials, with limestone and gypsum exhibiting comparatively fine distributions, while clinker was shifted toward larger particle sizes.

Figure 3.2 Particle Size Distribution of Raw Materials (PSD)

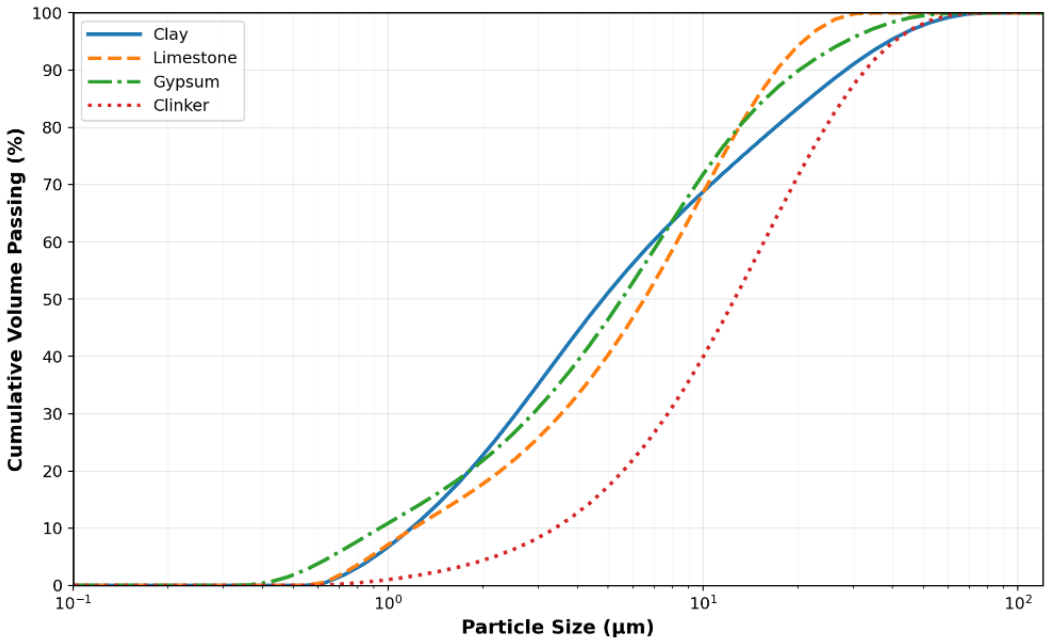

Table 3.2 Characteristic Particle Size Distribution of Raw Materials (µm)

(µm)	Clay	Limestone	Gypsum	Clinker
D10	1.4	1.4	1.1	3.9
D50	5.5	7.5	6.3	14.5
D90	32.5	19.6	23.2	37.5
D[4,3]	11.9	9.2	9.8	18.1

3.2.4 Aggregate and Chemical Admixture

The aggregate blend was prepared by combining five sand fractions with nominal particle size ranges of 2–3, 1–2, 0.5–1, 0.2–0.5, and 0.1–0.3 mm in proportions of 10, 20, 30, 20, and 20% by mass, respectively. These proportions corresponded to 500, 1000, 1500, 1000, and 1000 g for a 5 kg aggregate blend. The sand fractions were used as received from the supplier, without additional drying or moisture conditioning. Figure 3.3 presents the particle size distribution of the resulting blend together with the higher and lower grading limits for fine aggregate specified in ASTM C33/C33M [36].

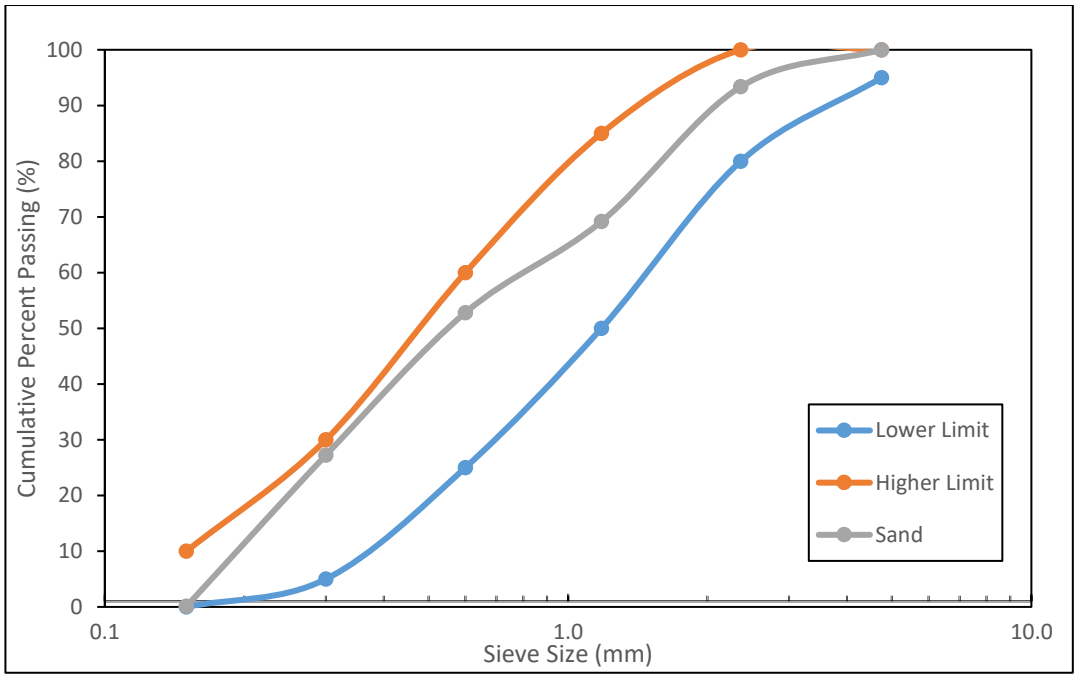

Figure 3.3 Particle Size Distribution of the Aggregate Blend Compared with the Fine Aggregate Grading Limits Specified in ASTM C33/C33M [36].

A polycarboxylate ether (PCE)-based superplasticizer MasterGlenium SKY 608 (Master Builders Solutions) with a density of 1.06–1.10 kg/L at 20 °C, was used to improve the workability of the LC³ mortars. The dosage was varied from 0 to 2 wt.% of binder [30]. The superplasticizer was added at a fixed dosage of 1.0% by mass of binder to all LC³ mixtures, including the uncalcined-clay reference mixture. Superplasticizer was not added to the OPC reference mortar. The dosage refers to the mass of the commercial liquid product.

3.3 Calcination Procedure

The raw clay was thermally activated using two calcination routes: a high-flux solar simulator coupled with a rotary reactor and a conventional laboratory muffle furnace. Before calcination, the raw clay was dried at 40 °C for 24 h and subsequently processed in a laboratory ball mill for 20 min to break up agglomerates formed during moist storage. The purpose of this treatment was to obtain a dispersed feed material for calcination rather than to deliberately reduce the size of the individual

mineral particles. The same preparation procedure was applied to the clay used in both calcination routes.

For each calcination route, six nominal temperatures 550, 600, 650, 700, 750, and 800 °C. Two holding periods 0.5 and 2 h were investigated. This resulted in twelve calcination conditions per route. The temperature and holding-time combinations were selected to examine the progression of clay transformation and its influence on the performance of the resulting LC³ mortars.

3.3.1 Solar Calcination

The solar calcination experiments were conducted using the high-flux solar simulator (HFSS) at the German Aerospace Center (DLR) in Cologne, Germany. The facility comprises ten xenon short-arc lamps and has a reported maximum thermal power capacity of 20 kW at the focal plane [29].

Previous work by Pasabeyoglu et al. investigated solar-assisted kaolin calcination using a high-flux solar simulator coupled with a batch-operated rotary reactor, with the calcined products subsequently evaluated for zeolite synthesis [9]. In the present study, solar-calcined clay was instead evaluated as a constituent of LC³. Figure 2.4 shows the simulator and reactor arrangement. The simulator mimicked concentrated solar power (CSP) systems using an artificial light source, allowing experiments to be conducted independently of outdoor weather conditions.

The rotary kiln reactor was operated in batch mode: approximately 1 kg of clay was loaded before each test, with no continuous feeding or discharge during calcination. Figure 3.4 presents the reactor configuration and a cross-sectional view. The reactor had an aperture diameter of 80 mm and an internal crucible made of high-temperature steel (grade 1.4828), with a diameter of 209 mm and a total length of 650 mm. Thermal insulation blankets were placed between the crucible and the outer Shell. About 1.25 L of material (~1 kg of clay) was used per batch.

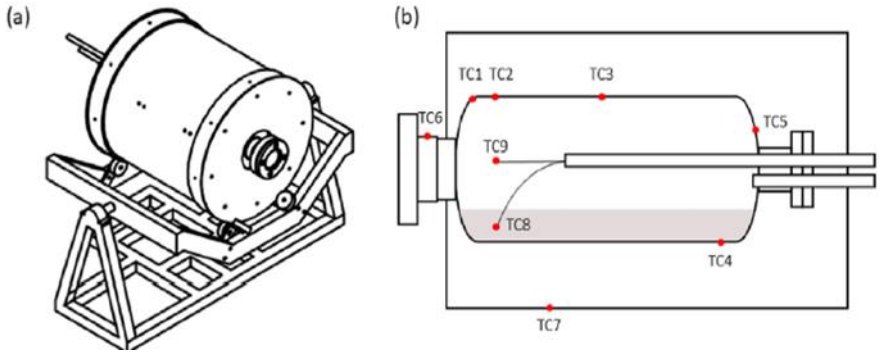

Figure 3.4 (a) Schematic diagram of the solar reactor and (b) construction of the tubular reactor with thermocouples (TC) [9].

Nine type-K thermocouples (TC1–TC9) were used to monitor temperatures at different locations within and around the reactor. (see Figure 3.4b). In the reactor configuration described by Pasabeyoglu et al., TC1–TC5 were positioned at axial distances of 28, 60, 230, 420, and 470 mm from the inlet, respectively. TC6 was located at the aperture and TC7 at the reactor housing. TC8 and TC9 were positioned approximately 60 mm from the inlet to measure the particle-bed and gas temperatures, respectively [9]. In the present experiments, TC3 served as the reference for reaching and maintaining the nominal target temperature, whereas TC8, which was in direct contact with the clay bed, was used to assess the material temperature. The nominal treatment temperature therefore refers to the TC3 reading, while the clay-bed temperature was monitored separately using TC8.

The kiln was loaded with 1 kg of kaolin and rotated at 3 rpm. Heating was gradually applied using up to seven lamps (5.6 kW). When the target temperature (monitored by TC3) was reached, it was maintained for 0.5 or 2 hours. Afterward, the lamps were switched off and the material was cooled.

The prepared clay was calcined in the solar reactor at nominal target temperatures of 550, 600, 650, 700, 750, and 800 °C, with holding periods of 0.5 and 2 h, resulting in 12 treatment conditions. The nominal target temperature and holding period were defined using TC3 as the reference. TC8, positioned in direct contact with the clay bed, was used to characterize the measured material temperature separately from the

nominal target temperature. A representative temperature profile for 600°C – 0.5 h holding period condition is presented in Figure 3.5.

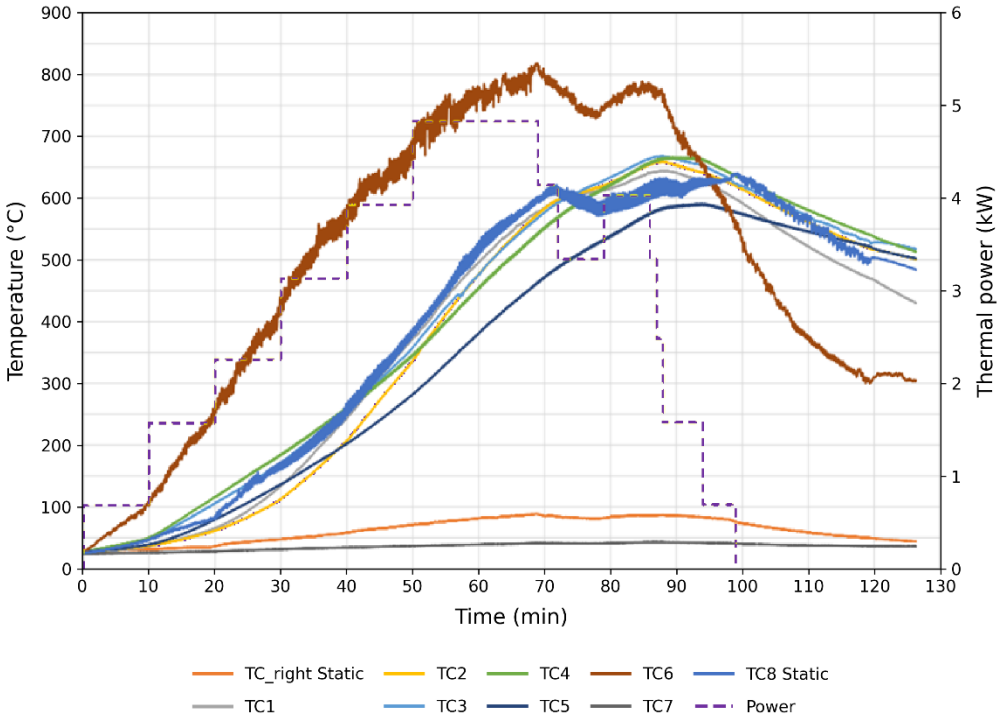

Figure 3.5 Temperature and thermal power profiles during solar calcination at a nominal target temperature of 600 °C with a holding period of 0.5 h.

3.3.2 Furnace Calcination

Conventional furnace calcination was performed in a laboratory muffle furnace at Middle East Technical University. Each batch consisted of approximately 0.5 kg of prepared clay placed in a ceramic crucible. The furnace was programd with a heating rate of 10 °C/min, and the clay remained stationary during treatment.

The same nominal temperature and holding-time combinations used in the solar program were adopted for furnace calcination. Two type-K thermocouples were used to monitor the temperatures during furnace calcination. TC1 was positioned at the centre of the clay bed, while TC2 was located within the furnace chamber. Their positions are illustrated in Figure 3.6. The heating and holding stages were controlled

by the furnace program. The prescribed holding period began when the furnace controller reached the target temperature, rather than when TC1 reached that temperature. For example, in the 800 °C–2 h program, the furnace was programd to reach 800 °C, maintain this temperature for 2 h, and subsequently discontinue heating to allow cooling.

Figure 3.8 presents the recorded temperature profiles for the nominal 800 °C–2 h condition, with the heating, holding, and cooling stages indicated. The remaining recorded furnace temperature profiles are provided in the Apendix B.

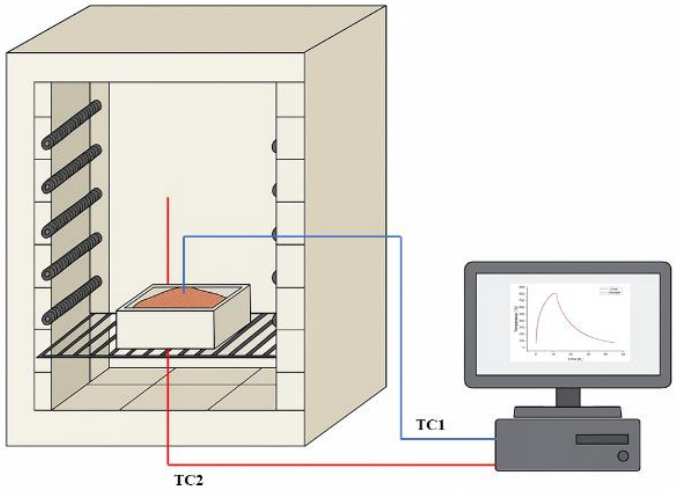

Figure 3.6 Schematic Diagram of the Furnace Setup

Figure 3.7 Laboratory Furnace and Temperature - Monitoring Setup Used for Clay Calciation at Middle East Techinal University

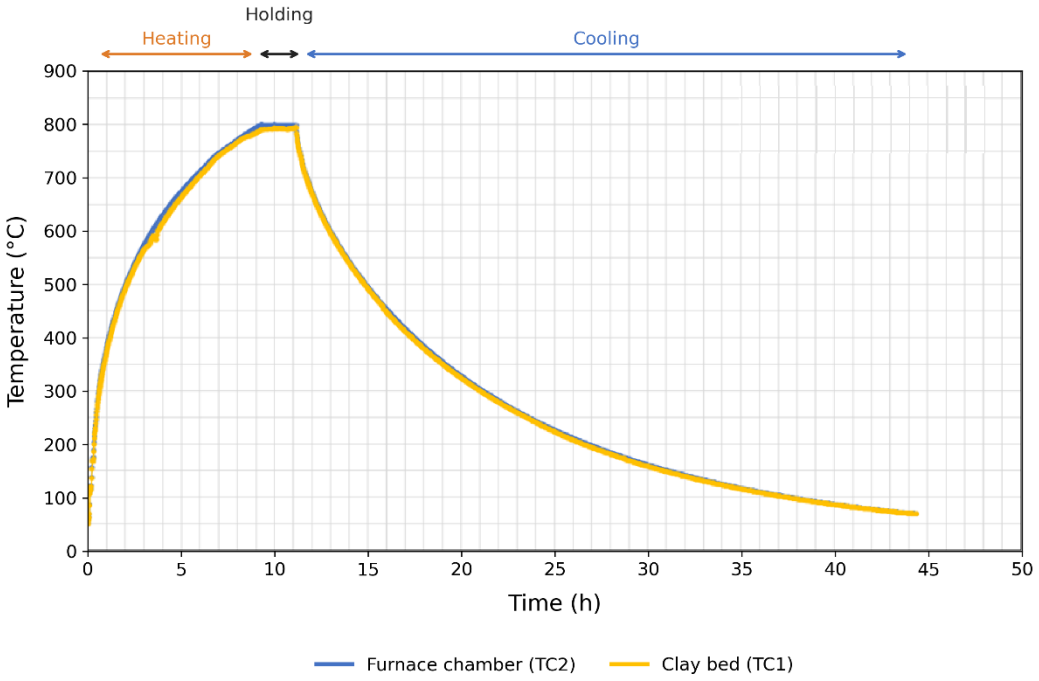

Figure 3.8 Temperature Profile Recorded During Furnace Calcination at 800°C for 2 hours

The two routes used the same source clay and nominal temperature–holding-time matrix. However, the batch mass, heat supply, reactor configuration, and material movement differed. Solar treatment used approximately 1 kg of clay in a rotating reactor, whereas furnace treatment used approximately 0.5 kg in a stationary ceramic crucible.

The comparison evaluates the calcined products obtained using two experimental setups that differed in batch mass, heat supply, reactor configuration, and material movement, while using the same nominal calcination temperatures and holding times.

The evolution of color of calcined clays with increasing temperature and duration, are represented in Figure 3.9. The photographs illustrate the general appearance of the samples and were not used for quantitative colour assessment.

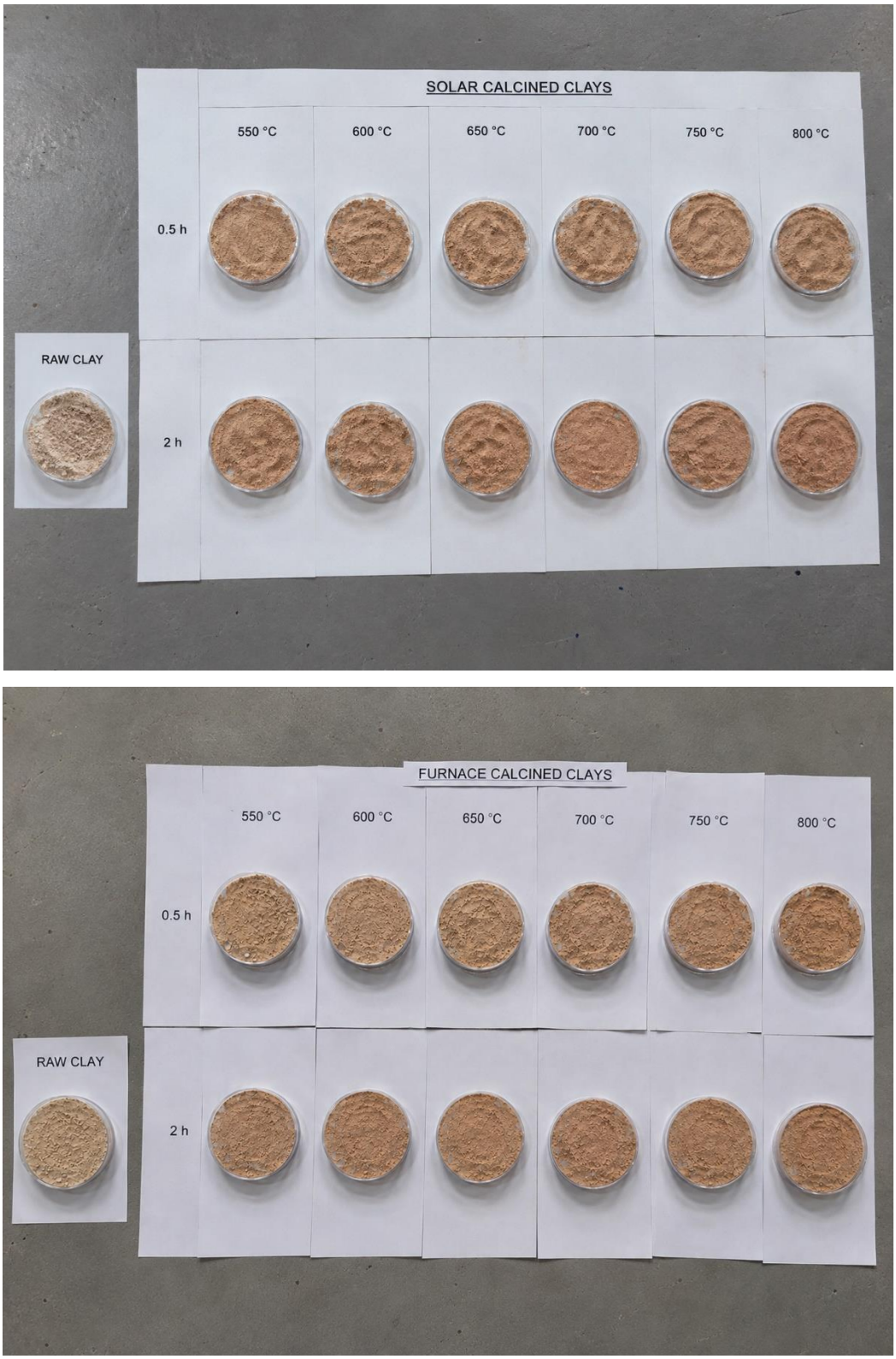

Figure 3.9 Color change of calcined clays

3.4 X-Ray Diffraction Analysis

X-ray diffraction (XRD) analyses were conducted on the raw materials and calcined clays to identify their crystalline phases and investigate mineralogical changes associated with thermal treatment. Measurements were performed at the Central Laboratory of Middle East Technical University using a Rigaku MiniFlex 600 diffractometer.

The instrument was operated at a tube voltage of 40 kV and a tube current of 15 mA. Diffraction data were collected over a 2θ range of 3–90°, with a step width of 0.02° and a scanning speed of 5°/min. The resulting patterns were analysed using HighScore Plus software for qualitative phase identification.

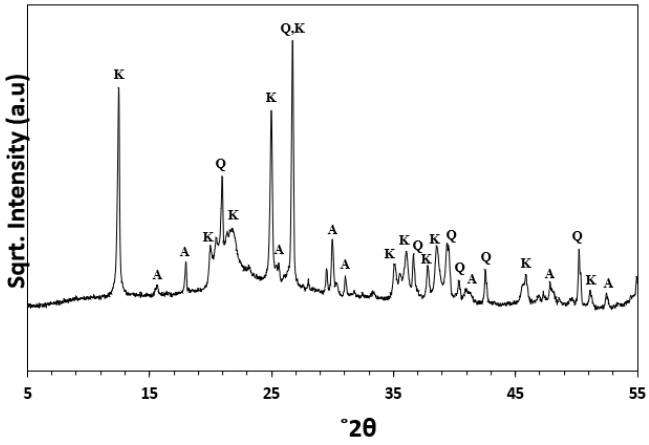

Figure 3.10 XRD Patterns of the Raw Materials (Q: Quartz COD 96-901-2601, K: Kaolinite COD 96-900-9231, A: Alunite COD 96-900-0035)

The diffraction patterns of the raw clay were compared with those of the furnace-calcined and solar-calcined clays to examine changes in the characteristic mineral reflections at different calcination temperatures and holding times.

3.5 Thermogravimetric Analysis

Thermogravimetric analysis (TGA), together with derivative thermogravimetry (DTG), was used to investigate the thermal decomposition of the raw clay and to establish a reference for evaluating the effects of calcination. Measurements were performed at the Central Laboratory of Middle East Technical University using an SDT 650 simultaneous TGA–DSC instrument under a nitrogen atmosphere over a temperature range of 25–1200 °C, at a heating rate of 10 °C/min. The TGA curve describes the change in sample mass during heating, whereas the DTG curve identifies the temperature regions in which mass loss occurs most rapidly. The TGA and DTG curves of the raw clay are presented in Figure 3.11.

For the investigated kaolinite–alunite clay, interpretation of the thermal response required consideration of overlapping decomposition processes. Alunite dehydroxylation can occur within the same temperature region as kaolinite dehydroxylation; therefore, attributing the entire mass loss in this region to kaolinite could overestimate its content. Mohammadi and Salarirad reported an alunite dehydroxylation interval of approximately 508–577 °C for the ore investigated in their study and summarized earlier studies reporting an interval of approximately 450–550 °C [25].

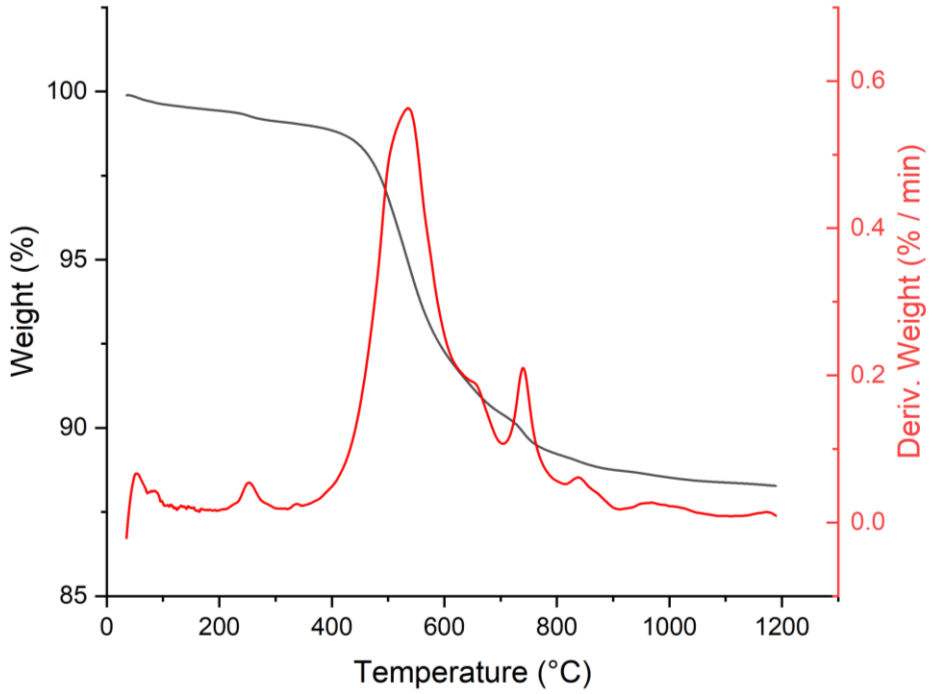

Figure 3.11. TGA/DTG curves of raw clay

Gaussian peak deconvolution was performed in Origin to distinguish overlapping contributions within the raw-clay DTG curve. Five Gaussian components were fitted with fixed peak centres at approximately 252, 501, 537, 657, and 739 °C, while their widths and areas were allowed to vary during fitting. The cumulative fit yielded a coefficient of determination of $R^2 = 0.992$, indicating close overall agreement between the fitted and experimental curves. The individual components were interpreted using the XRD results and thermal decomposition behaviour reported in the literature.

An initial low temperature mass loss event appeared at ~63 °C due to surface water desorption [31]. At ~252 °C, mass loss was linked to interlayer water or residual organics [31]. The component centred at 252 °C was tentatively attributed to dehydration. The literature summarized by Mohammadi and Salarirad places dehydration within approximately 50-240 °C [25].

The overlapping components at 501 and 537 °C were attributed to K-alunite and kaolinite dehydroxylation, respectively. The proposed alunite contribution is consistent with the dehydroxylation intervals discussed above [31]. Kaolinite dehydroxylation involves the removal of structural hydroxyl groups and the formation of metakaolin [23]. Separating these two contributions was particularly important for estimating the mass loss associated with kaolinite. However, their fitted areas remain dependent on the baseline, peak model, and constraints used during deconvolution.

The components centred at 657 and 739 °C were associated with the multistep desulphation of alunite-derived decomposition products. Both components fall within the broader interval of approximately 600–830 °C reported for this process [25]. They were therefore interpreted as separate contributions within the higher-temperature decomposition region, without assigning each peak to a specific intermediate phase.

The deconvoluted DTG curve is presented in Figure 3.12. The peak centres, areas, and proposed thermal processes are summarized in Table 3.3, while the complete Origin fitting report is provided in the Apendix A.

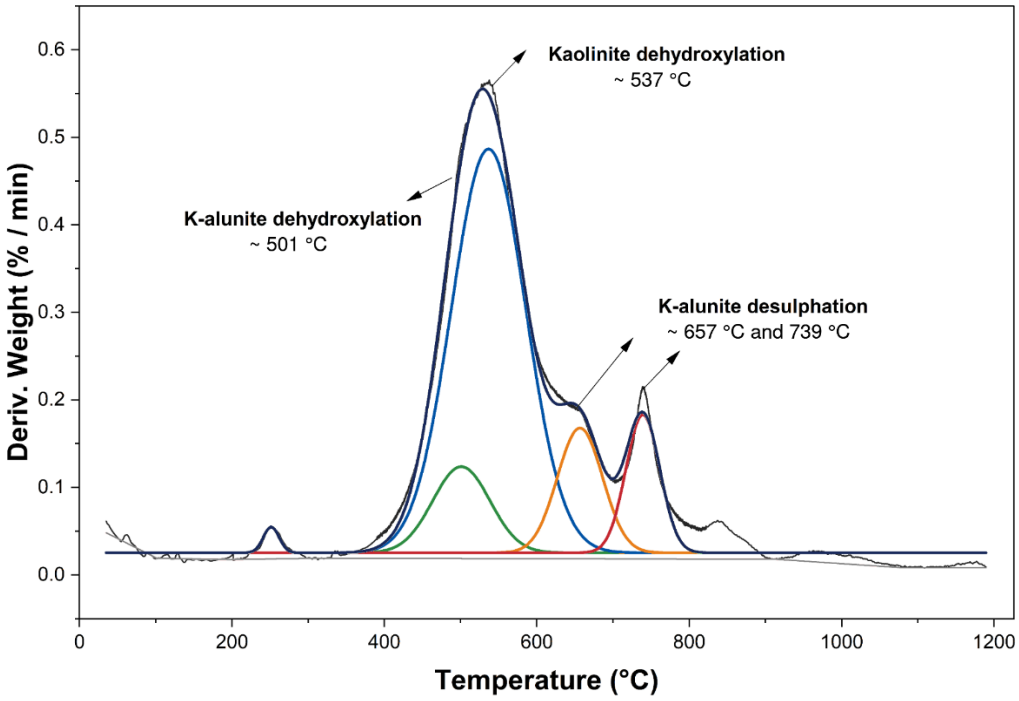

Figure 3.12 Deconvolution analysis on raw clay

Table 3.3 DTG Analysis with Gauss Model

Peak	**Thermal Process**	**Peak centre, x_c(°C)**	**Peak area, A(%·°C·min⁻¹)**
1	Dehydration	251.50	0.76 ± 0.01
2	K-alunite Dehydroxylation	501.04	9.25 ± 0.07
3	Kaolinite Dehydroxylation	536.72	56.38 ± 0.09
4	K-alunite Desulphation	656.67	10.61 ± 0.04
5	K-alunite Desulphation	739.19	8.83 ± 0.02

To estimate the initial kaolinite content of the raw clay, the mass loss from dehydroxylation was used with the deconvolution analysis on origin. Using the fitted kaolinite peak area of 56.38 %·°C·min⁻¹ and the TGA heating rate of 10 °C/min, the corresponding dehydroxylation mass loss was calculated as 5.638 wt.%. This yielded an estimated kaolinite content of approximately 40.4 wt. %, conditional on the proposed peak assignment and the separation of the overlapping dehydroxylation

contributions. The values obtained from the Table 3.3 and calculations followed this equation [4].

$$(wt\%_{Kaolinite}) = (wt\%_{kaol-OH})\, x \frac{M_{Kaolinite}}{2M_{H_2O}} \quad (3.1)$$

$$(wt\%_{Kaolinite}) = \left(\frac{peak\ area}{heating\ rate}\right) x \frac{258.16}{36.03} \quad (3.2)$$

$$= \left(\frac{56.38\ °C\ \%/min}{10\ °C/min}\right) x \frac{258.16}{36.03} = 40.40\ \%$$

This helped establish a baseline for evaluating the degree of kaolinite conversion during calcination. Here, M_{kaolin} and M_{H_2O} represent the molar masses of kaolinite and water, respectively.

3.6 Mixture Proportions of OPC and LC³ Mortars

The mixture proportions of the LC³ (both conventional furnace-calcined and solar-calcined) specimens formulated within the scope of this thesis were based on the standard LC³ – 50 formulation (50% Clinker, 30% Calcined Clay, 15% Limestone, and 5% Gypsum), which is widely reported to provide a good balance between mechanical performance and CO_2 reduction [1, 11, 32] In order to maximize the synergistic reaction between metakaolin and calcium carbonate, promoting the formation of strength-enhancing carboaluminate phase, the mass ratio of calcined clay to limestone was 2:1 [4, 32]. The nominal water-to-binder (w/b) ratio was maintained at 0.50 based on the added mixing water. The superplasticizer was premixed with a portion of this water before being introduced into the mortar; no additional dilution water was used. The water contained in the liquid superplasticizer itself was not deducted from the mixing-water quantity and the aggregate-to-binder mass ratio was set at 3.0 [33]. To compensate for the loss of workability induced by the characteristically high specific surface area of the calcined clay, and to achieve a fresh-state consistency comparable to that of the ordinary Portland cement (OPC) reference baseline, a polycarboxylate ether (PCE) based superplasticizer was

incorporated into the LC³ mixtures at a dosage of 1.0% by total weight of the binder system, based on compatibility studies available in the literature [34]. The batch quantities were selected to provide sufficient mortar to fill three 40 × 40 × 160 mm prism molds. Each batch contained 484 g of binder. A polycarboxylate ether-based superplasticizer (PCE-SP) was added at a fixed dosage of 4.84 g per batch, corresponding to 1.0% of the total binder mass, to all calcined-clay mixtures and the raw-clay reference mixture. This dosage refers to the commercial liquid product as supplied. No superplasticizer was added to the OPC reference mortar. In the raw-clay reference mixture, the calcined clay was replaced with an equal mass of uncalcined clay to evaluate the influence of thermal activation. The mixture proportions are presented in Table 3.4.

Table 3.4 Mixture (Proportions) of OPC, LC³ and Raw-Clay Reference Mortars

Specimen	**Composition (g)**						
	w/b	Clinker	Calcined Clay	Limestone	Gypsum	Water	Aggregate
OPC	0.5	459.80	-	-	24.20	242.0	1452.0
SLC³-50 **FLC³-50** **Raw Clay**	0.5	242.00	145.20	72.60	24.20	242.0	1452.0

All mixtures had a nominal water-to-binder mass ratio of 0.50 and a sand-to-binder mass ratio of 3.00. For the raw-clay reference mixture, the quantity listed under "Calcined Clay" represents uncalcined clay.

3.7 Mortar Preparation and Testing

The mortar mixtures described in Section 3.6 were evaluated through fresh-state consistency measurements and mechanical testing. The flow-table test was used to assess mortar flowability, while flexural and compressive strength tests were used to evaluate strength development at different curing ages.

3.7.1 Fresh Mortar Consistency

The consistency of the fresh mortars was evaluated using the flow-table test, with ASTM C1437-20 adopted as the reference procedure [35]. Measurements were used to assess the flow behaviour of the mixtures prepared at the selected water-to-binder ratio and to examine the effect of superplasticizer addition.

The mortar was placed into the flow mould in two layers and compacted. After filling, the excess mortar was removed and the surface was levelled. The mould was then lifted, and the flow table was subjected to 25 drops within 15 s. The resulting mortar spread was used to evaluate fresh-state consistency.

Representative photographs of the mortar mixtures prepared with and without superplasticizer are presented in Figure 3.13. These photographs illustrate the observed differences in spread, while quantitative comparisons should be based on the measured flow values.

Figure 3.13 The flow characteristics of the LC^3 with and without superplasticizer for 600 °C - 0.5h duration.

3.7.2 Specimen Preparation and Curing

Fresh mortar was cast into 40 × 40 × 160 mm prism moulds in two approximately equal layers. After 24 h, the specimens were demoulded and transferred to a curing room, where they were maintained under humid conditions until testing at 2, 7, and 28 days.

3.7.3 Mechanical Testing

The mechanical performance of the mortar mixtures was evaluated through flexural and compressive strength tests at curing ages of 2, 7, and 28 days. Testing was performed using a UTCM-3742 testing machine. The mechanical loading procedures followed ASTM C348-21 for flexural strength [37] and ASTM C349-24 [38] for compressive strength.

For each mixture and testing age, three 40 × 40 × 160 mm mortar prisms were tested in flexure. The six resulting prism halves were subsequently tested in compression. Flexural strength was reported as the mean of three measurements, while compressive strength was reported as the mean of six measurements. Standard deviations were calculated separately for each mixture, testing age, and test type and presented as error bars in the corresponding strength plots.

The test results were used to compare strength development among the OPC reference, the raw-clay reference, and the LC^3 mixtures produced with furnace-calcined and solar-calcined clays. Comparisons were made at corresponding curing ages to evaluate the influence of calcination route, temperature, and holding time within the adopted mixture composition.

CHAPTER 4

RESULTS AND DISCUSSION

4.1 Characterization of Raw and Calcined Clays

The raw and calcined clays were characterized to evaluate the mineralogical and thermal transformations occurring under different calcination conditions. X-ray diffraction (XRD) was used to monitor changes in the crystalline phases, particularly kaolinite, alunite, and quartz, whereas thermogravimetric and derivative thermogravimetric analyses (TGA/DTG) were employed to examine the associated thermal events and residual mass losses. The combined findings were used to compare furnace and solar calcination and to determine the influence of calcination temperature and holding time on the transformation of the clay.

4.1.1 Mineralogical Analysis by X-Ray Diffraction

The mineralogical transformations of the raw and calcined clays were investigated by XRD. Particular attention was given to the evolution of the kaolinite and alunite reflections, while quartz was monitored as a relatively stable crystalline phase. The effects of calcination temperature, holding time, and calcination method were evaluated comparatively.

Figure 4.1 presents the XRD patterns of the raw clay and the clays calcined in a conventional furnace between 550 and 800 °C for holding periods of 0.5 and 2 h. The raw clay contained kaolinite (K), alunite (A), and quartz (Q). The characteristic kaolinite reflections were observed at approximately 12.34° and 24.86° 2θ, while the main quartz reflection was identified at approximately 26.61° 2θ.

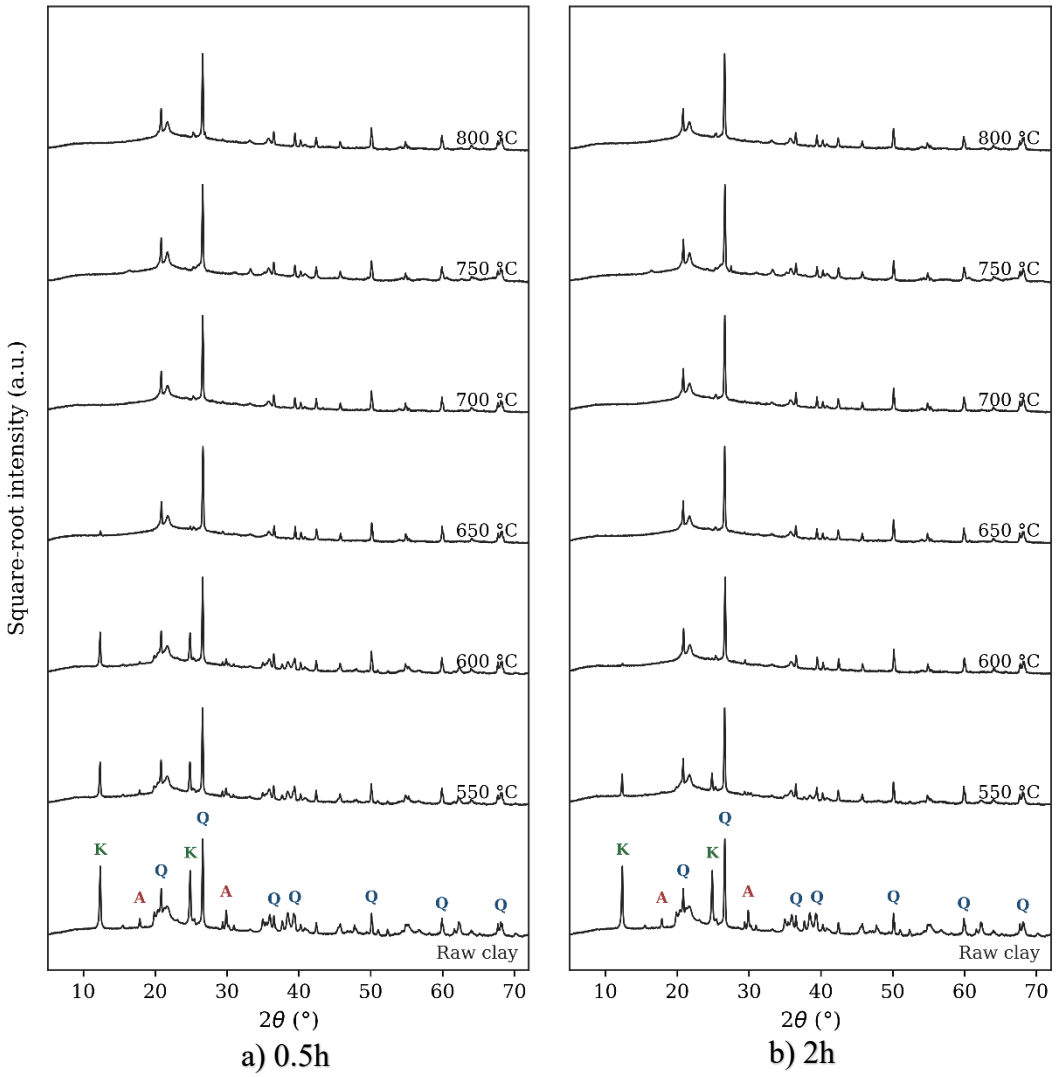

Figure 4.1 XRD patterns of the raw clay and furnace-calcined clays produced at different temperatures for a) 0.5 h and b) 2 h holding periods. K: kaolinite, A: alunite, and Q: quartz

For the furnace-calcined samples, the characteristic kaolinite reflections progressively weakened with increasing temperature and holding time. At 550 °C, these reflections remained visible after both 0.5 and 2h, indicating that a detectable fraction of crystalline kaolinite persisted. At 600 °C, the reflections were still evident after 0.5h but almost completely disappeared after 2h. A similar influence of holding time was observed at 650 °C: weak residual kaolinite reflections remained after 0.5 h, whereas no characteristic reflections were identified after 2h. No identifiable kaolinite reflections were observed in the samples treated between 700 and 800 °C.

These observations indicate that extending the holding period promoted the loss of kaolinite crystallinity at the intermediate furnace temperatures. The disappearance of the characteristic reflections is consistent with the structural transformation associated with dehydroxylation and metakaolin formation [23]. The XRD analysis was qualitative and was used to identify changes in detectable crystalline phases. It did not quantify phase contents, amorphous content, or the degree of conversion, nor did it independently establish pozzolanic reactivity..

The characteristic alunite reflections also weakened and eventually became unidentifiable as the furnace treatment temperature and holding time increased. This indicates the transformation of the original crystalline alunite phase, although the diffraction patterns alone do not establish the identity or quantity of all resulting decomposition products. Quartz reflections remained clearly identifiable throughout the furnace series, showing that crystalline quartz persisted under the investigated conditions.

Figure 4.2 presents the XRD patterns of the raw clay and the clays calcined using solar energy between 550 and 800 °C for holding periods of 0.5 and 2 h.

Following solar calcination, the characteristic kaolinite reflections largely disappeared even at a nominal temperature of 550 °C and a holding time of 0.5 h. No clearly identifiable kaolinite reflections were observed at higher treatment temperatures or longer holding periods. The loss of these reflections, together with the broad background observed in the aluminosilicate region, is consistent with the formation of a poorly crystalline product following kaolinite dehydroxylation. The amorphous content was not quantified in this analysis.

Alunite reflections also decreased considerably after solar treatment, indicating changes in its original crystalline structure. Quartz reflections remained identifiable across the solar series. Thus, both calcination routes altered the kaolinite- and alunite-bearing components while retaining detectable crystalline quartz.

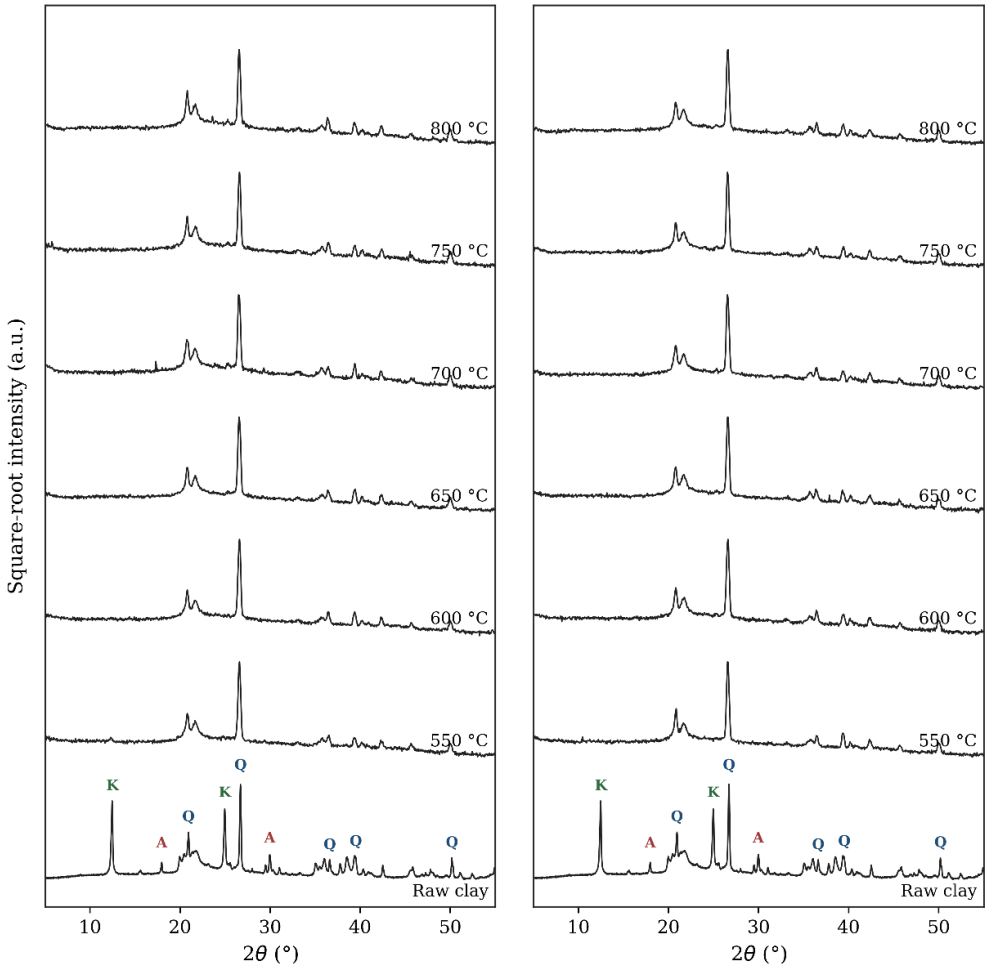

Figure 4.2 XRD patterns of the raw clay and the clays calcined using solar Energy produced at different temperatures for a) 0.5 h and (b) 2 h holding periods. K: kaolinite, A: alunite, and Q: quartz

Comparison of the two series indicates that the characteristic kaolinite reflections became largely unidentifiable under milder nominal treatment conditions in the solar system. At 550 °C, residual kaolinite reflections remained visible in the furnace-calcined samples at both holding periods, whereas they largely disappeared in the solar-calcined sample after 0.5 h. At higher temperatures, the two routes produced broadly similar qualitative outcomes with respect to the disappearance of identifiable kaolinite reflections.

This comparison should be interpreted in terms of the nominal temperature and holding time used for each treatment. Matching these parameters does not

necessarily imply identical temperature histories throughout the clay, particularly because the two systems differ in their heating arrangements and heat-transfer conditions. The XRD results therefore demonstrate a difference in the observed mineralogical response under the investigated operating conditions, without identifying a unique mechanism responsible for that difference.

The results support the ability of solar thermal treatment to produce mineralogical changes comparable to those achieved by conventional furnace calcination. However, the disappearance of crystalline reflections alone does not necessarily indicate higher pozzolanic reactivity; therefore, these results should be evaluated together with the thermal analysis and mechanical performance of the calcined clays

4.1.2 Thermal Analysis by TGA/DTG

Following the mineralogical evaluation by XRD, TGA and DTG were used to examine the residual thermal decomposition of the raw and calcined clays. The TGA curves describe the mass losses occurring during analytical heating, whereas the DTG curves help distinguish the overlapping thermal events. Here, residual mass loss refers to the mass lost during the TGA measurement after the preceding calcination treatment, rather than the mass removed during calcination itself. This distinction provides the basis for comparing the thermal response of the raw clay with those of the furnace-calcined and solar-calcined samples.

Figure 4.3 and Figure 4.4 present the TGA curves of the raw clay and the solar- and furnace-calcined samples, respectively. The raw clay exhibited the greatest mass loss, while the calcined samples generally showed progressively lower residual mass losses with increasing calcination temperature. Longer holding periods also generally reduced the subsequent mass loss. These trends indicate that a greater proportion of the thermally decomposable constituents had already undergone transformation during the preceding treatment.

Both calcination routes exhibited this overall behaviour. However, the total residual mass loss cannot be interpreted exclusively as a measure of unconverted kaolinite because the investigated clay also contains alunite and exhibits additional thermal decomposition events. Consequently, the TGA trends were evaluated together with the DTG profiles and the revised deconvolution of the raw clay.

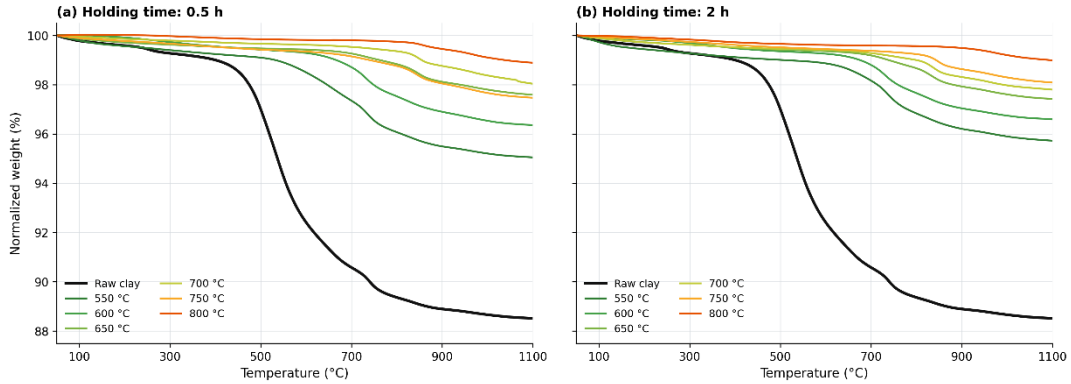

Figure 4.3 TGA Curves of raw and solar-calcined clays

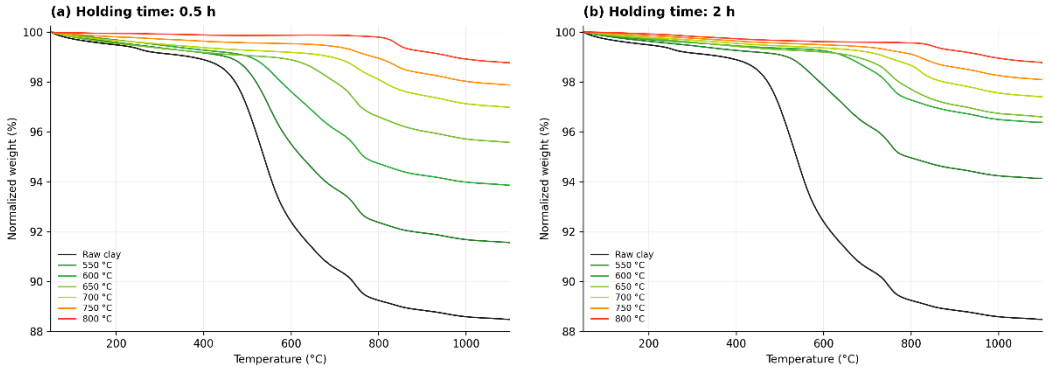

Figure 4.4 TGA Curves of raw and furnace-calcined clays

The raw-clay deconvolution, presented in Figure 3.12 and Table 3.3, resolved five components centred at 252, 501, 537, 657, and 739 °C. The first component was tentatively associated with dehydration. The overlapping components at 501 and 537 °C were attributed to K-alunite and kaolinite dehydroxylation, respectively, while the higher-temperature components were associated with desulphation of alunite-

derived decomposition products. The inclusion of the component near 501 °C is important because alunite dehydroxylation can overlap the temperature region commonly associated with kaolinite transformation [25].

Separating the overlapping alunite and kaolinite contributions yielded an estimated initial kaolinite content of approximately 40.4 wt.%, as described in Section 3.5. This estimate depends on the proposed peak assignments and the separation of the overlapping DTG components. Figure 4.5 and Figure 4.6 present the DTG curves of the solar- and furnace-calcined clays, respectively. Following calcination, the thermal response in the overlapping kaolinite–alunite dehydroxylation region was substantially reduced relative to that of the raw clay. Residual events were generally more evident after treatment at lower temperatures and became less pronounced with increasing calcination temperature and holding time. These observations support the occurrence of substantial dehydroxylation during both calcination routes.

Nevertheless, the residual response in this region cannot be assigned entirely to kaolinite. A contribution from alunite-related transformations may remain, particularly where the corresponding events overlap. The reduction in this response should therefore be interpreted together with the persistence or disappearance of the characteristic kaolinite reflections in XRD. For the furnace series, the progressive weakening of these reflections with temperature and holding time is consistent with the general reduction in residual dehydroxylation. For the solar series, the largely unidentifiable kaolinite reflections likewise support substantial structural transformation, while DTG provides complementary information on the remaining thermally decomposable constituents.

The higher-temperature DTG features were interpreted with reference to the raw-clay components at 657 and 739 °C. Their association with alunite-derived decomposition products is consistent with the broader multistep desulphation behaviour reported in the literature [25]. Residual events in this region therefore should not be interpreted as evidence of unconverted kaolinite. Their decreasing

prominence with more intensive calcination indicates that the preceding thermal treatment also affected the accompanying alunite-bearing constituents.

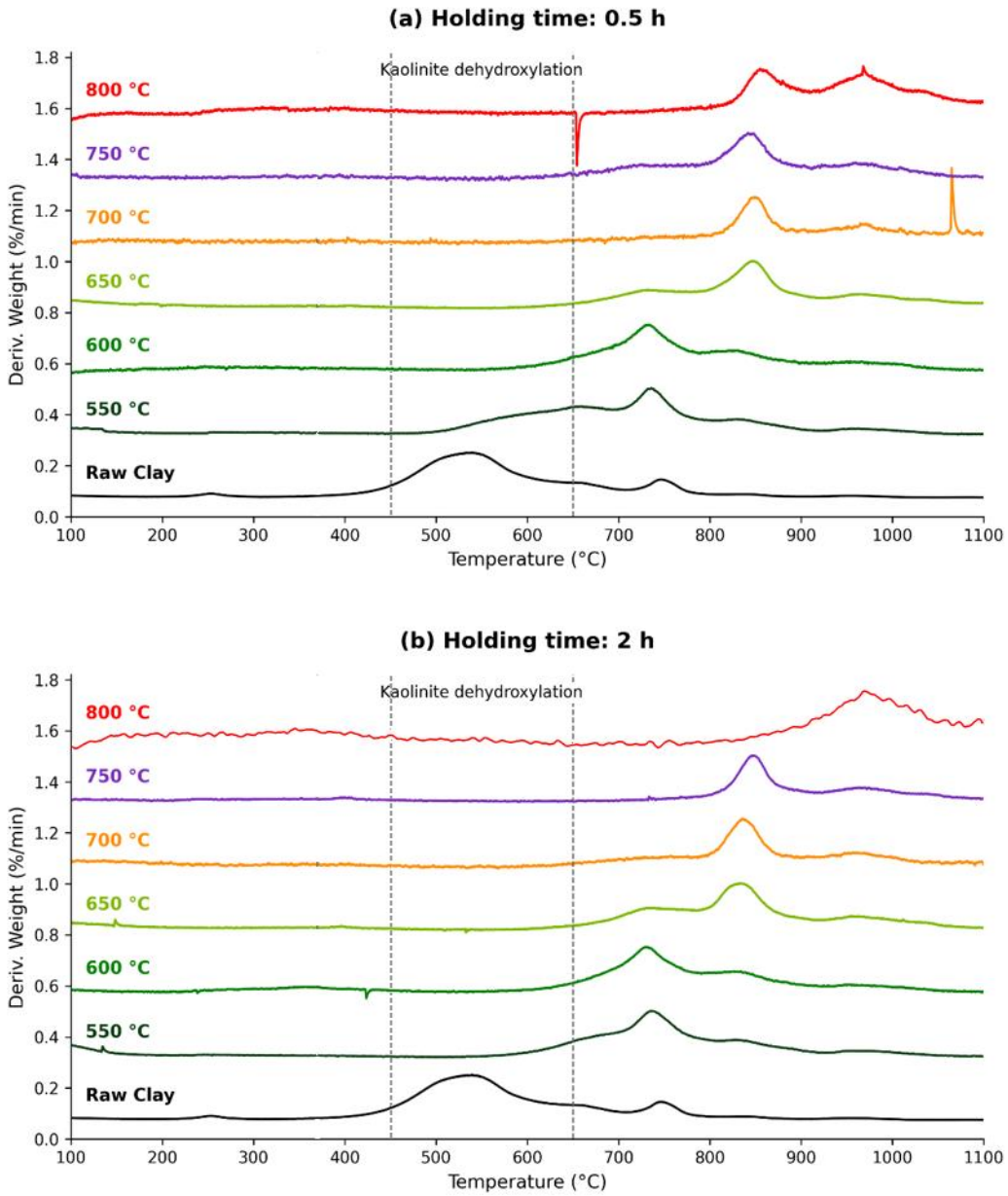

Figure 4.5 DTG curves of solar-calcined clays at different calcination temperatures for (a) 0.5 h and (b) 2 h. (Curves vertically offset for clarity)

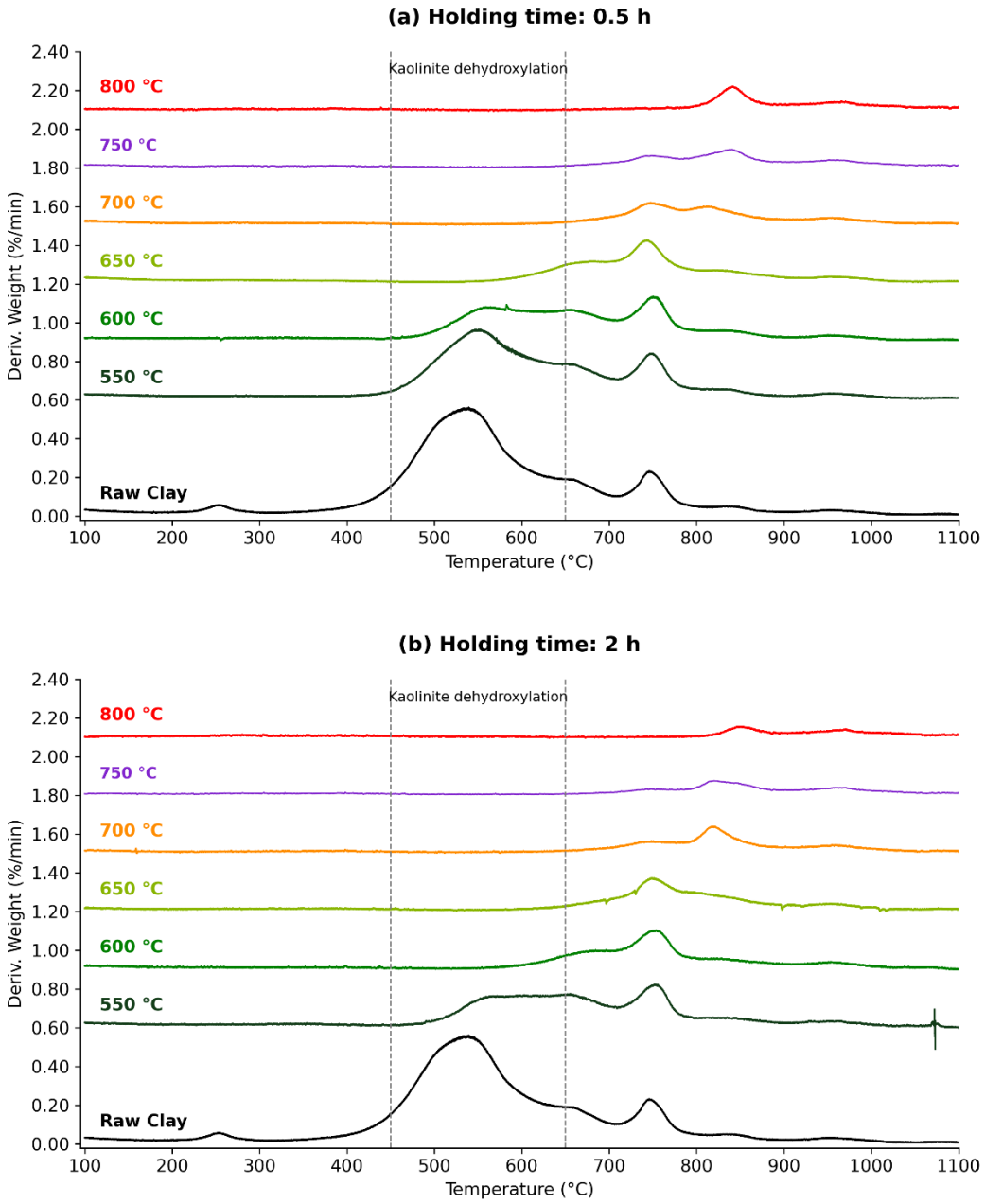

Figure 4.6 DTG curves of furnace-calcined clays at different calcination temperatures for (a) 0.5 h and (b) 2 h. (Curves vertically offset for clarity)

At nominal calcination temperatures of 550–600 °C, the solar-calcined samples exhibited lower residual dehydroxylation signals than the furnace-calcined samples, suggesting more extensive dehydroxylation during solar treatment. At higher calcination temperatures, the responses of the two routes became more similar.

Increasing temperature and holding time generally reduced the residual decomposition response, consistent with the mineralogical changes observed by XRD. This supports the ability of both routes to thermally activate the investigated clay, although it does not establish identical degrees of transformation at every corresponding nominal treatment condition.

A lower residual mass loss does not, by itself, identify the calcination condition producing the highest mortar strength. The thermal measurements describe the extent and character of the remaining decomposition processes, while the mechanical tests assess the performance of the resulting material within the adopted LC³-50 mixture. The strength results are therefore examined subsequently to determine how the observed mineralogical and thermal changes relate to engineering performance.

4.2 Flexural Strength

The flexural strengths of the LC³ mortars after 2, 7, and 28 days of curing are presented in Table 4.1. Results are reported as the mean and sample standard deviation of three prism measurements for each mixture and testing age. The OPC control and the mixture containing uncalcined clay were included as reference mixtures.

At 2 days, all mixtures containing calcined clay exhibited lower mean flexural strengths than the OPC control, which reached 4.43 ± 0.06 MPa. Mean strengths ranged from 3.00 to 3.83 MPa for furnace-calcined mixtures and from 2.70 to 3.73 MPa for solar-calcined mixtures. By 7 days, several mixtures from both calcination routes exceeded the OPC mean of 5.43 ± 0.12 MPa. At 28 days, most calcined-clay mixtures also exceeded the OPC mean of 5.27 ± 0.12 MPa, with strengths ranging from 5.13 to 6.47 MPa for furnace-calcined mixtures and from 4.80 to 7.10 MPa for solar-calcined mixtures.

Neither increasing calcination temperature nor extending holding time produced a consistent increase in flexural strength across the investigated conditions. The solar-

calcined mixture treated at 700 °C for 0.5 h exhibited a lower mean strength at 28 days than at 7 days, together with comparatively large scatter at 28 days (4.80 ± 1.31 MPa). Similarly, the solar-calcined mixture treated at 800 °C for 2 h exhibited a 7-day flexural strength of 3.77 ± 1.33 MPa, only slightly above its 2-day value. These irregularities and the relatively large scatter may reflect specimen-related defects or variability introduced during specimen preparation and testing. However, the available results do not establish specimen defects as the cause of the observed behaviour. The raw-clay reference reached 7.40 ± 0.20 MPa at 28 days, exceeding the means of all calcined-clay mixtures. The flexural results therefore did not reproduce the consistent benefit of thermal activation observed relative to the raw-clay reference in the 28-day compressive-strength results.

Table 4.1 Flexural Strength values for both SLC³ and FLC³ and reference mixtures at 2, 7 and 28 days

Method	Calcination temperature (°C)	Holding time (h)	2 days	7 days	28 days
FLC³	550	0.5	3.57 ± 0.67	5.23 ± 0.21	5.83 ± 0.49
FLC³	600	0.5	3.83 ± 0.06	5.13 ± 0.25	5.67 ± 0.29
FLC³	650	0.5	3.80 ± 0.17	5.30 ± 0.26	5.20 ± 0.53
FLC³	700	0.5	3.80 ± 0.10	4.90 ± 0.46	6.33 ± 0.25
FLC³	750	0.5	3.67 ± 0.15	5.20 ± 0.10	5.67 ± 0.15
FLC³	800	0.5	3.00 ± 0.26	4.70 ± 0.20	5.13 ± 0.12
SLC³	550	0.5	3.73 ± 0.15	5.93 ± 0.25	7.10 ± 0.46
SLC³	600	0.5	3.27 ± 0.06	5.23 ± 0.40	6.43 ± 0.81
SLC³	650	0.5	3.40 ± 0.20	4.73 ± 0.23	6.40 ± 0.10
SLC³	700	0.5	3.00 ± 0.36	5.87 ± 0.38	4.80 ± 1.31
SLC³	750	0.5	3.53 ± 0.21	5.00 ± 0.17	6.37 ± 0.35
SLC³	800	0.5	3.23 ± 0.15	5.60 ± 0.35	5.93 ± 0.55
FLC³	550	2	3.83 ± 0.06	4.93 ± 0.35	6.07 ± 0.31
FLC³	600	2	3.60 ± 0.36	5.87 ± 0.32	6.10 ± 0.61
FLC³	650	2	3.27 ± 0.25	5.50 ± 0.20	5.67 ± 0.15
FLC³	700	2	3.70 ± 0.00	5.57 ± 0.40	6.30 ± 0.53
FLC³	750	2	3.67 ± 0.21	5.80 ± 0.30	6.47 ± 0.55
FLC³	800	2	3.67 ± 0.15	5.03 ± 0.21	6.10 ± 0.36
SLC³	550	2	2.80 ± 0.10	5.53 ± 0.21	6.03 ± 0.21
SLC³	600	2	3.20 ± 0.26	4.73 ± 0.32	6.30 ± 0.17
SLC³	650	2	2.70 ± 0.26	5.67 ± 0.25	6.07 ± 0.51
SLC³	700	2	3.27 ± 0.40	5.07 ± 0.25	6.30 ± 0.20
SLC³	750	2	3.27 ± 0.15	5.60 ± 0.56	6.23 ± 0.78
SLC³	800	2	3.70 ± 0.10	3.77 ± 1.33	6.50 ± 0.36
OPC	—	—	4.43 ± 0.06	5.43 ± 0.12	5.27 ± 0.12
Raw clay	—	—	3.27 ± 0.12	4.77 ± 0.25	7.40 ± 0.20

Values are mean ± standard deviation (MPa), FLC³: furnace-calcined clay mortar; SLC³: solar-calcined clay mortar.

4.3 Compressive Strength

The compressive strength of the LC³ mortars was evaluated after 2, 7, and 28 days of curing are presented in Table 4.2. The experimental program included furnace- and solar-calcined clays treated at nominal temperatures of 550–800 °C for holding times of 0.5 and 2 h. The OPC control was used as the principal strength benchmark, while the mixture containing uncalcined clay provided an additional reference for evaluating the contribution of thermal activation.

Table 4.2 Compressive Strength values for both SLC³ and FLC³ and reference mixtures at 2, 7 and 28 days

Method	Calcination temperature (°C)	Holding time (h)	2 days	7 days	28 days
FLC³	550	0.5	15.17 ± 0.15	27.08 ± 0.42	29.30 ± 1.42
FLC³	600	0.5	16.93 ± 0.71	33.30 ± 0.17	33.50 ± 2.11
FLC³	650	0.5	16.90 ± 0.20	30.90 ± 0.79	33.30 ± 0.36
FLC³	700	0.5	15.07 ± 0.80	30.70 ± 1.05	35.15 ± 1.88
FLC³	750	0.5	14.48 ± 0.31	30.03 ± 1.56	35.03 ± 1.80
FLC³	800	0.5	12.30 ± 0.62	28.40 ± 0.53	33.77 ± 1.65
SLC³	550	0.5	14.87 ± 0.15	32.00 ± 1.21	36.13 ± 2.15
SLC³	600	0.5	12.53 ± 0.27	27.90 ± 1.52	37.72 ± 3.29
SLC³	650	0.5	12.85 ± 0.40	28.10 ± 1.05	39.35 ± 2.68
SLC³	700	0.5	12.23 ± 0.22	30.40 ± 0.10	38.60 ± 3.50
SLC³	750	0.5	14.73 ± 0.17	32.00 ± 0.36	38.27 ± 0.76
SLC³	800	0.5	13.87 ± 0.12	34.65 ± 1.29	37.33 ± 0.15
FLC³	550	2	16.72 ± 0.89	32.93 ± 1.40	33.95 ± 1.81
FLC³	600	2	15.22 ± 0.13	34.18 ± 1.23	34.88 ± 3.07
FLC³	650	2	15.60 ± 0.70	32.12 ± 1.83	35.63 ± 1.42
FLC³	700	2	15.37 ± 0.34	34.60 ± 2.05	36.85 ± 1.32
FLC³	750	2	14.33 ± 0.32	33.67 ± 1.38	37.95 ± 0.58
FLC³	800	2	15.12 ± 0.17	32.53 ± 0.31	39.15 ± 1.98
SLC³	550	2	11.38 ± 0.10	28.57 ± 1.31	36.33 ± 0.56
SLC³	600	2	13.10 ± 0.10	28.58 ± 2.00	36.78 ± 1.53

Table 4.2 Compressive Strength values for both SLC³ and FLC³ and reference mixtures at 2, 7 and 28 days

Method	Calcination temperature (°C)	Holding time (h)	2 days	7 days	28 days
SLC³	650	2	11.50 ± 0.10	29.43 ± 2.50	37.98 ± 1.83
SLC³	700	2	12.58 ± 0.25	29.07 ± 0.67	39.23 ± 0.45
SLC³	750	2	13.57 ± 0.39	30.97 ± 0.85	38.63 ± 0.86
SLC³	800	2	15.47 ± 0.39	35.57 ± 1.28	40.55 ± 1.89
OPC	—	—	21.08 ± 0.49	31.78 ± 0.72	37.30 ± 1.36
Raw clay	—	—	11.47 ± 0.16	21.13 ± 0.61	25.62 ± 0.55

Values are mean ± standard deviation (MPa). FLC³: furnace-calcined clay mortar; SLC³: solar-calcined clay mortar

4.3.1 Compressive Strength at 2 Days

Figure 4.7 present the 2-day compressive strengths of LC³ mortars containing furnace- and solar-calcined clays treated for 0.5 and 2 h, respectively. All mixtures containing calcined clay exhibited lower mean compressive strengths than the OPC control, which reached 21.08 ± 0.49 MPa. The furnace-calcined mixtures developed strengths of 12.30–16.93 MPa, whereas the solar-calcined mixtures reached 11.38–15.47 MPa. These ranges indicate that neither calcination route enabled the investigated LC³ mixtures to match the early-age strength of the OPC control.

The raw-clay reference developed a compressive strength of 11.47 ± 0.16 MPa. Most mixtures containing calcined clay exhibited higher mean strengths than this reference. However, the solar-calcined mixtures treated at 550 and 650 °C for 2 h remained close to the raw-clay result, with mean strengths of 11.38 and 11.50 MPa, respectively. The early-age benefit associated with thermal activation therefore varied with the treatment condition.

Neither increasing the nominal calcination temperature nor extending the holding time produced a consistent increase in 2-day strength across both calcination routes. The lower 2-day strengths observed in this study are consistent with the reduced

clinker content of LC³ and the progressive contribution of calcined-clay reactions to strength development. Replacing clinker with calcined clay and limestone reduces the amount of clinker available for early hydration, while the resulting strength also depends on the reactivity and physical characteristics of the replacement materials. Although calcined clay can contribute to hydration at early ages, its contribution continues to develop with curing. Literature reports that suitably formulated LC³-50 mixtures can achieve strengths comparable to Portland cement from approximately 7 days [4]. Accordingly, the lower strengths measured here at 2 days suggest that the contributions of the replacement materials had not yet sufficiently compensated for the reduced clinker content.

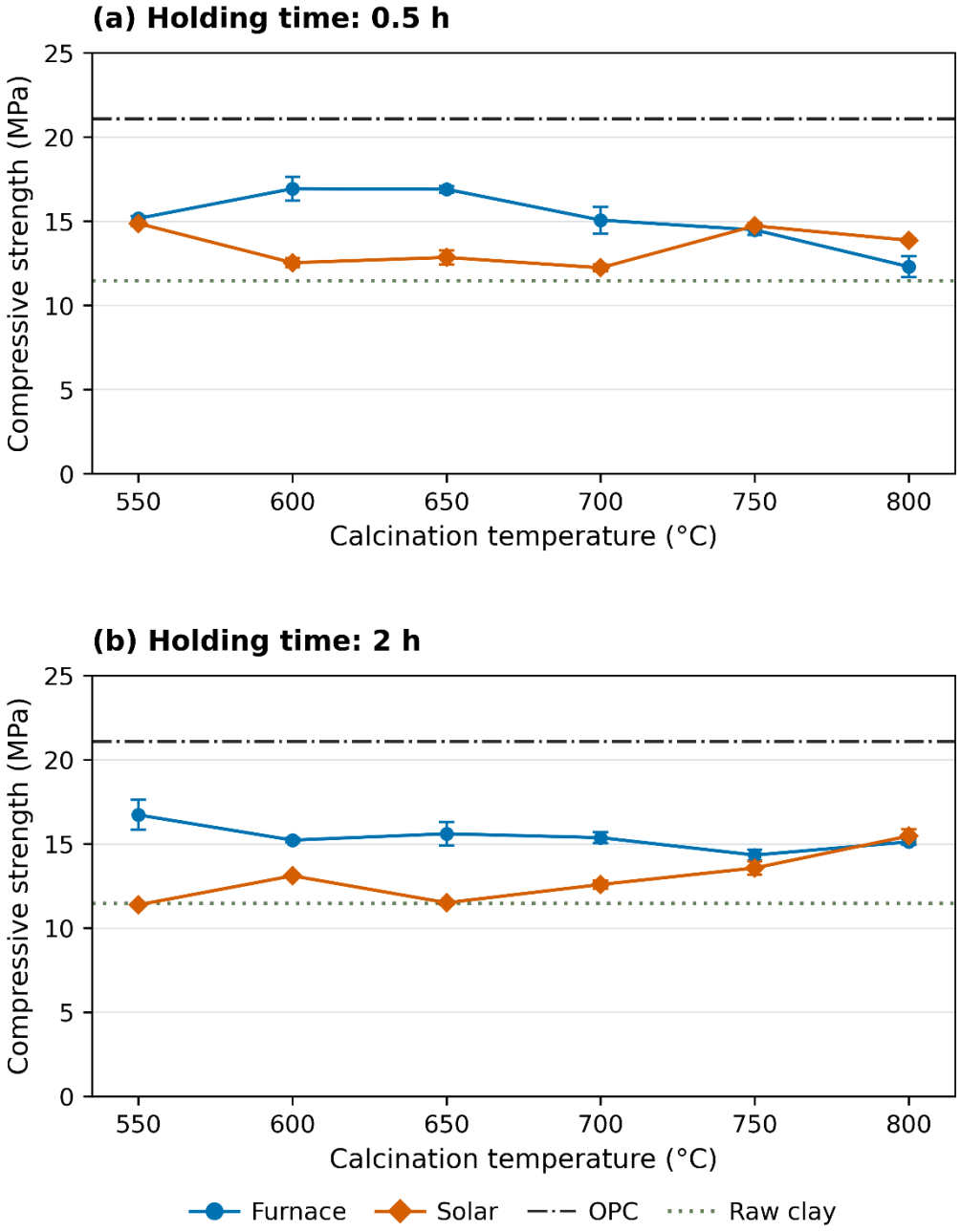

Figure 4.7 Compressive Strength at 2 days of LC³ Mortars Incorporating Furnace- and Solar-Calcined Clays at Holding Times of (a) 0.5 h and (b) 2 h.

Error bars represent ± one standard deviation. Horizontal lines indicate the mean strengths of the OPC and raw-clay references.

4.3.2 Compressive Strength at 7 Days

Figure 4.8 present the corresponding 7-day compressive strengths for holding times of 0.5 and 2 h, respectively. At this age, all mixtures exhibited increased mean compressive strength compared with their corresponding 2-day results. The OPC control reached 31.78 ± 0.72 MPa, while the raw-clay reference developed a strength of 21.13 ± 0.61 MPa. The furnace-calcined mixtures exhibited mean strengths ranging from 27.08 to 34.60 MPa, whereas the solar-calcined mixtures ranged from 27.90 to 35.57 MPa. All mixtures containing calcined clay therefore exceeded the mean strength of the raw-clay reference, and several also reached or exceeded the OPC control mean.

For the furnace-calcined mixtures, the mean strength at 600 °C–0.5 h was 33.30 ± 0.17 MPa, exceeding the OPC reference. All mixtures prepared with clay furnace-calcined for 2 h also exhibited mean strengths above the OPC control, ranging from 32.12 to 34.60 MPa. These observations indicate that several furnace-calcination conditions enabled the LC^3 mixtures to overcome the strength deficit relative to OPC observed at 2 days.

For the solar-calcined mixtures, the 550 °C–0.5 h and 750 °C–0.5 h conditions both produced mean strengths of 32.00 MPa, close to the OPC control mean of 31.78 MPa. At 800 °C, the mean strengths were 34.65 ± 1.29 MPa after a holding time of 0.5 h and 35.57 ± 1.28 MPa after 2 h. These results demonstrate that LC^3 produced with solar-calcined clay could also attain or exceed the measured OPC mean strength by 7 days under selected treatment conditions.

The principal development between 2 and 7 days was therefore the transition from all calcined-clay mixtures remaining below the OPC control to several mixtures achieving comparable or higher mean strengths.

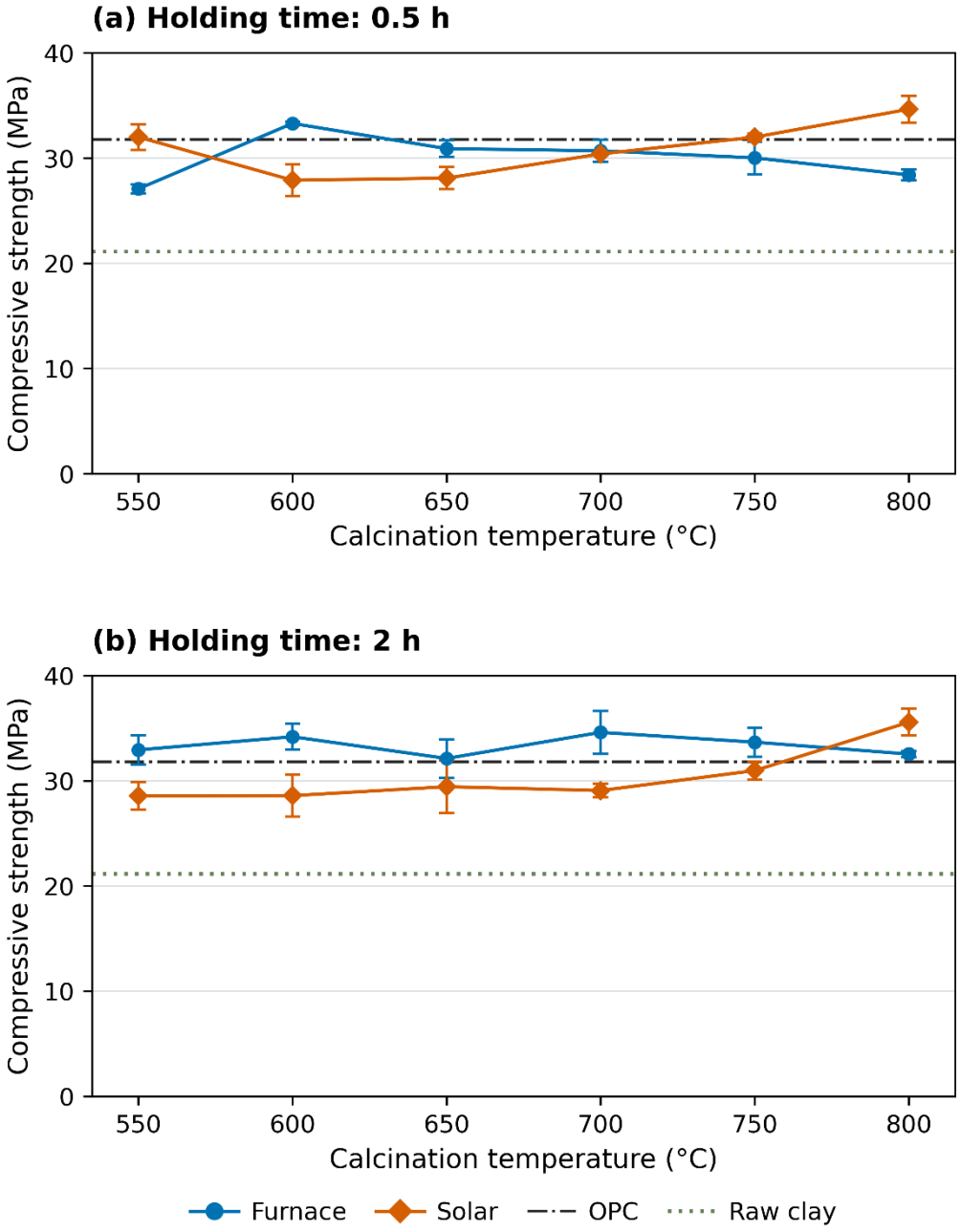

Figure 4.8 Compressive Strength at 7 days of LC³ Mortars Incorporating Furnace- and Solar-Calcined Clays at Holding Times of (a) 0.5 h and (b) 2 h.

Error bars represent ± one standard deviation. Horizontal lines indicate the mean strengths of the OPC and raw-clay references.

4.3.3 Compressive Strength at 28 Days

Figure 4.9 present the 28-day compressive strengths for holding times of 0.5 and 2 h, respectively. The OPC control reached a compressive strength of 37.30 ± 1.36 MPa, while the raw-clay reference developed a strength of 25.62 ± 0.55 MPa. The furnace-calcined mixtures exhibited mean strengths ranging from 29.30 to 39.15 MPa, whereas the solar-calcined mixtures ranged from 36.13 to 40.55 MPa. All mixtures containing calcined clay exceeded the mean strength of the raw-clay reference.

For the furnace-calcined mixtures, the mean strengths obtained after a holding time of 0.5 h remained below the OPC reference, ranging from 29.30 to 35.15 MPa. In the 2 h series, the mixture treated at 700 °C reached 36.85 ± 1.32 MPa, close to the OPC control mean. The mixtures treated at 750 and 800 °C exhibited mean strengths above the reference, reaching 37.95 ± 0.58 and 39.15 ± 1.98 MPa, respectively. Thus, selected furnace-calcination conditions enabled the LC^3 mixtures to attain mean strengths comparable to or above that of the OPC control at 28 days.

For the solar-calcined mixtures, the mean strengths obtained at 600–800 °C in the 0.5 h series and at 650–800 °C in the 2 h series were at or above the OPC control mean. The remaining solar mixtures developed mean strengths of 36.13–36.78 MPa, also close to the reference value. At 800 °C–0.5 h, the result of 37.33 ± 0.15 MPa was nearly identical to the OPC mean, while the corresponding 2 h mixture reached 40.55 ± 1.89 MPa. These results show that solar-calcined clay could be incorporated into LC^3 mixtures that achieved the OPC strength benchmark under several of the investigated treatment conditions.

28 day results support the feasibility of producing LC^3 with solar-calcined clay that achieves compressive strengths comparable to those obtained using conventionally furnace-calcined clay and that meets or exceeds the measured OPC mean under selected conditions.

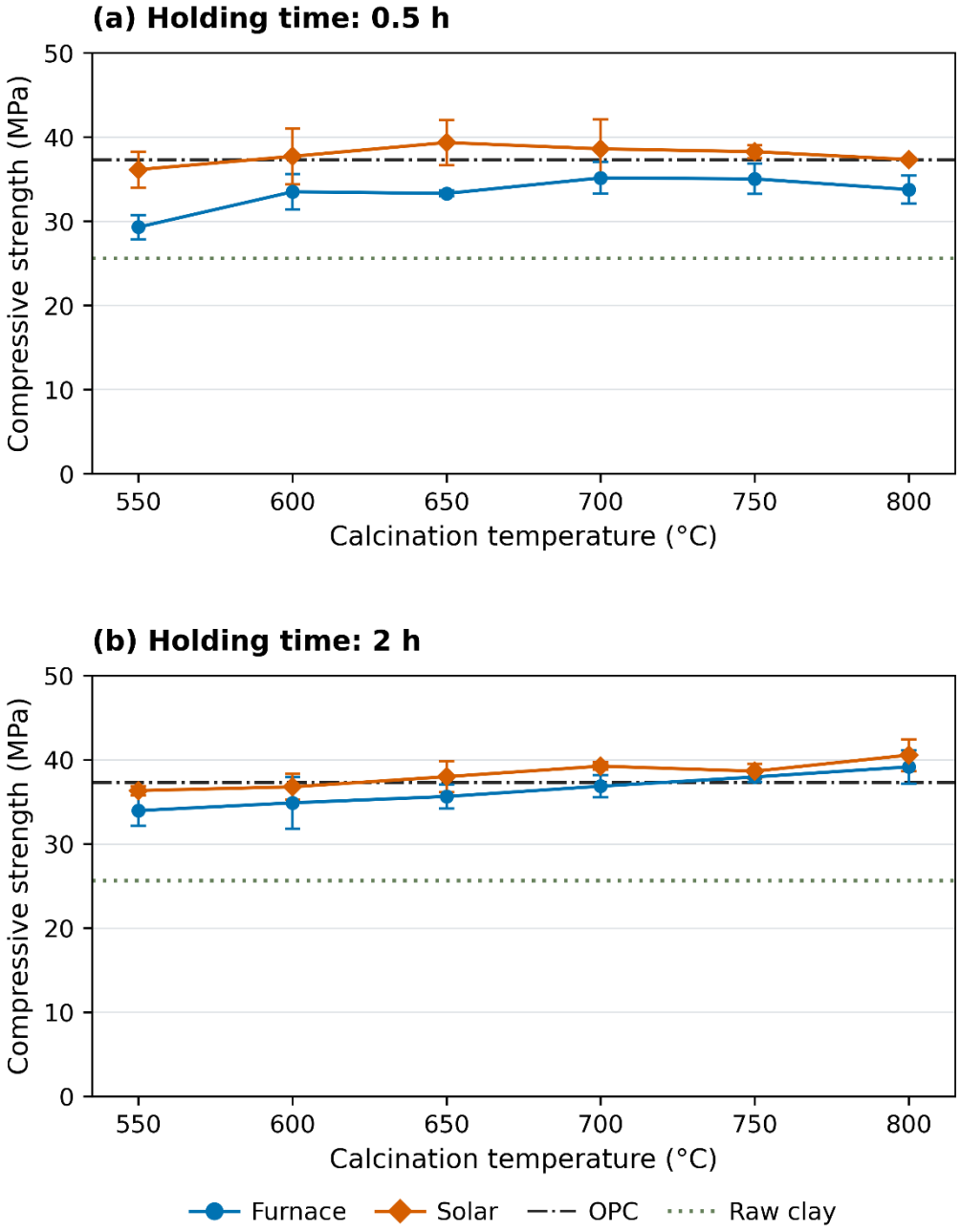

Figure 4.9 Compressive Strength at 28 days of LC³ Mortars Incorporating Furnace- and Solar-Calcined Clays at Holding Times of (a) 0.5 h and (b) 2 h.

Error bars represent ± one standard deviation. Horizontal lines indicate the mean strengths of the OPC and raw-clay references.

4.4 Combined Evaluation of XRD, TGA/DTG and Compressive Strength

The XRD, TGA/DTG, and compressive-strength results provide complementary evidence regarding the thermal activation of the investigated kaolinite–alunite clay. XRD was used to examine changes in detectable crystalline phases, while TGA/DTG provided information on the thermal decomposition of the raw clay and the residual thermal events in the calcined samples. Compressive-strength testing was used to evaluate the mechanical performance of LC^3 mortars incorporating these calcined products. Considering these measurements together allows the mineralogical and thermal changes to be assessed in relation to the observed mechanical performance.

The mechanical results demonstrate that the strength contribution associated with thermal activation developed with curing age. At 2 days, all investigated LC^3 mixtures remained below the OPC control mean. By 7 days, several furnace- and solar-calcined mixtures attained mean strengths close to or above the OPC reference. At 28 days, all mixtures containing calcined clay exceeded the raw-clay reference mean, while selected conditions from both calcination routes also exceeded the OPC mean. These observations establish a mechanical benefit associated with calcination within the investigated binder system, without requiring individual treatment conditions to be ranked on the basis of small differences in mean strength.

The combined results also show that the reduction of kaolinite reflections or residual dehydroxylation does not, by itself, establish the resulting mortar strength. The relationship between mineralogical transformation and mechanical performance was not represented by a consistent increase in strength with nominal calcination temperature or holding time. Accordingly, the XRD and TGA/DTG observations should be interpreted alongside the strength measurements rather than used individually to identify an optimum treatment.

Comparisons between the two calcination routes should also distinguish nominal treatment conditions from the actual thermal history experienced by the clay. Matching nominal temperatures and holding times does not establish identical

temperature histories throughout the samples. However, the present results do not isolate the contribution of individual heat-transfer or temperature-distribution effects to the observed strength differences. Likewise, specific mechanisms such as sintering or changes in surface area cannot be established from the available measurements.

Results support the technical feasibility of using solar-calcined clay in LC^3 mortars that attain mean compressive strengths close to or above the OPC reference under selected treatment conditions. This conclusion concerns the observed performance within the experimental program; it does not establish statistical equivalence between calcination routes or demonstrate a reduction in energy consumption or environmental impact.

CHAPTER 5

CONCLUSION AND RECOMMENDATIONS

5.1 Summary and Conclusion

This study investigated the technical feasibility of using solar-calcined kaolinite–alunite clay as a constituent of limestone calcined clay cement (LC^3). A locally sourced clay was treated using a high-flux solar simulator coupled with a rotary reactor and a conventional laboratory muffle furnace. The experimental program covered nominal calcination temperatures of 550–800 °C and holding periods of 0.5 and 2 h. Mineralogical and thermal changes were examined using XRD and TGA/DTG, while the compressive strength of mortars prepared with a fixed LC^3-50 composition was evaluated after 2, 7, and 28 days. Portland cement and raw-clay-containing mortars were included as reference mixtures.

Based on the experimental findings, the following conclusions were drawn:

1. The raw clay contained kaolinite, alunite, and quartz. Its thermal response therefore reflected overlapping mineral transformations rather than kaolinite decomposition alone. Gaussian deconvolution of the raw-clay DTG curve included components assigned to alunite and kaolinite dehydroxylation at approximately 501 and 537 °C, respectively. The fitted kaolinite contribution yielded an estimated initial kaolinite content of approximately 40.4 wt.%. This estimate depends on the adopted peak assignments and the separation of the overlapping thermal contributions.

2. Both calcination routes produced substantial changes in the mineralogical characteristics of the clay. In the furnace series, characteristic kaolinite reflections progressively weakened with increasing temperature and holding time and became unidentifiable at the higher treatment temperatures. In the

solar series, these reflections largely disappeared even at a nominal temperature of 550 °C after 0.5 h. Quartz remained detectable across both series. These observations support the disruption of the kaolinite structure, although qualitative XRD alone does not quantify amorphous content or establish pozzolanic reactivity.

3. The thermal analyses complemented the XRD observations. Calcined samples generally exhibited lower residual mass losses and less pronounced dehydroxylation-related events than the raw clay, indicating that thermal decomposition had already occurred during calcination. However, the overlapping contributions of kaolinite and alunite prevented the entire residual mass loss in the dehydroxylation region from being attributed exclusively to unconverted kaolinite.

4. At 2 days, all LC³ mixtures containing calcined clay exhibited lower mean compressive strengths than the OPC control, which reached 21.08 MPa. Furnace-calcined mixtures developed mean strengths of 12.30–16.93 MPa, while solar-calcined mixtures reached 11.38–15.47 MPa. Most calcined-clay mixtures exceeded the raw-clay reference mean of 11.47 MPa, although the improvement was limited under some treatment conditions. Thus, calcination did not enable the investigated LC³ mixtures to match the OPC strength at this early age.

5. By 7 days, all calcined-clay mixtures exceeded the raw-clay reference mean of 21.13 MPa. Mean strengths ranged from 27.08 to 34.60 MPa for furnace-calcined mixtures and from 27.90 to 35.57 MPa for solar-calcined mixtures. Several conditions from both routes attained mean strengths close to or above the OPC control value of 31.78 MPa. The early strength deficit relative to OPC therefore decreased as curing progressed.

6. At 28 days, furnace-calcined mixtures developed mean compressive strengths of 29.30–39.15 MPa, while solar-calcined mixtures reached 36.13–40.55 MPa. All calcined-clay mixtures exceeded the raw-clay reference mean

of 25.62 MPa. Selected conditions from both routes also exceeded the OPC control mean of 37.30 MPa. These results demonstrate that solar-calcined clay could be incorporated into LC³-50 mortars achieving mean strengths close to or above the OPC benchmark within the investigated experimental program.

7. Neither increasing nominal calcination temperature nor extending the holding period produced a consistent increase in compressive strength across both routes and all curing ages. The reduction of kaolinite reflections and residual dehydroxylation therefore did not independently identify a single optimum treatment condition. Mineralogical and thermal observations must be considered together with the performance of the resulting mortar.

Findings support the technical feasibility of producing an LC³ precursor through solar aided calcination of the investigated clay. The comparison concerns the products obtained under the operating conditions of the two experimental systems. Matching nominal temperatures and holding periods did not establish identical thermal histories, and the observed strength results do not demonstrate statistical equivalence between the routes. The principal outcome is that solar treatment produced mineralogical and thermal changes consistent with clay activation and enabled selected LC³ mixtures to attain the OPC mean-strength benchmark at later curing ages.

5.2 Recommendations

Although the objectives of this study were successfully achieved, several aspects deserve further investigation to improve the understanding and practical application of LC³ systems produced with locally available clays.

- Quantitative phase analysis using Rietveld refinement, supported by an appropriate internal standard, should be conducted to quantify crystalline and

amorphous contents and complement the interpretation of kaolinite and alunite transformations.

- Advanced microstructural characterization techniques such as SEM/EDS, FTIR, BET surface area analysis, and mercury intrusion porosimetry (MIP) may be employed to better explain the relationship between pore structure, hydration products, and mechanical performance.
- The influence of different limestone fineness, gypsum content, clinker replacement ratios, and superplasticizer dosages should be optimized to further improve both fresh and hardened properties.
- Finally, Life cycle assessment (LCA) and operating-cost analysis should be conducted using measured energy consumption and material inputs. These assessments should compare furnace and solar calcination on a common production basis and distinguish the laboratory solar simulator from a system using direct concentrated sunlight.

REFERENCES

1. Scrivener, K., Martirena, F., Bishnoi, S., Maity, S.: Calcined clay limestone cements (LC3), (2018)

2. Juenger, M.C.G., Snellings, R., Bernal, S.A.: Supplementary cementitious materials: New sources, characterization, and performance insights, (2019)

3. Zunino, F., Scrivener, K.: The reaction between metakaolin and limestone and its effect in porosity refinement and mechanical properties. Cem. Concr. Res. 140, (2021). https://doi.org/10.1016/j.cemconres.2020.106307

4. Avet, F., Scrivener, K.: Investigation of the calcined kaolinite content on the hydration of Limestone Calcined Clay Cement (LC3). Cem. Concr. Res. 107, 124–135 (2018). https://doi.org/10.1016/j.cemconres.2018.02.016

5. Hanein, T., Thienel, K.C., Zunino, F., Marsh, A.T.M., Maier, M., Wang, B., Canut, M., Juenger, M.C.G., Haha, M. Ben, Avet, F., Parashar, A., Al-Jaberi, L.A., Almenares-Reyes, R.S., Alujas-Diaz, A., Scrivener, K.L., Bernal, S.A., Provis, J.L., Sui, T., Bishnoi, S., Martirena-Hernández, F.: Clay calcination technology: state-of-the-art review by the RILEM TC 282-CCL, (2022)

6. Moumin, G., Tescari, S., Sundarraj, P., de Oliveira, L., Roeb, M., Sattler, C.: Solar treatment of cohesive particles in a directly irradiated rotary kiln. Solar Energy. 182, 480–490 (2019). https://doi.org/10.1016/j.solener.2019.01.093

7. Krueger, K.R., Davidson, J.H., Lipiński, W.: Design of a new 45 kWe high-flux solar simulator for high-temperature solar thermal and thermochemical research. Journal of Solar Energy Engineering, Transactions of the ASME. 133, (2011). https://doi.org/10.1115/1.4003298

8. Petrasch, J., Coray, P., Meier, A., Brack, M., Häberling, P., Wuillemin, D., Steinfeld, A.: A novel 50 kW 11,000 suns high-flux solar simulator based on

an array of xenon arc lamps. Journal of Solar Energy Engineering, Transactions of the ASME. 129, 405–411 (2007). https://doi.org/10.1115/1.2769701

9. Pasabeyoglu, P., Moumin, G., de Oliveira, L., Roeb, M., Akata, B.: Solarization of the zeolite production: Calcination of kaolin as proof-of-concept. J. Clean. Prod. 414, (2023). https://doi.org/10.1016/j.jclepro.2023.137611

10. Fernandez, R., Martirena, F., Scrivener, K.L.: The origin of the pozzolanic activity of calcined clay minerals: A comparison between kaolinite, illite and montmorillonite. Cem. Concr. Res. 41, 113–122 (2011). https://doi.org/10.1016/j.cemconres.2010.09.013

11. Antoni, M., Rossen, J., Martirena, F., Scrivener, K.: Cement substitution by a combination of metakaolin and limestone. Cem. Concr. Res. 42, 1579–1589 (2012). https://doi.org/10.1016/j.cemconres.2012.09.006

12. Sarrión, B., Perejón, A., Sánchez-Jiménez, P.E., Amghar, N., Chacartegui, R., Manuel Valverde, J., Pérez-Maqueda, L.A.: Calcination under low CO2 pressure enhances the calcium Looping performance of limestone for thermochemical energy storage. Chemical Engineering Journal. 417, (2021). https://doi.org/10.1016/j.cej.2020.127922

13. Esence, T., Guillot, E., Tessonneaud, M., Sans, J.L., Flamant, G.: Solar calcination at pilot scale in a continuous flow multistage horizontal fluidized bed. Solar Energy. 207, 367–378 (2020). https://doi.org/10.1016/j.solener.2020.06.098

14. Ijaz, N., Ye, W.M., ur Rehman, Z., Ijaz, Z., Junaid, M.F.: Global insights into micro-macro mechanisms and environmental implications of limestone calcined clay cement (LC3) for sustainable construction applications, (2024)

15. Krishnan, S., Emmanuel, A.C., Shah, V., Parashar, A., Mishra, G., Maity, S., Bishnoi, S.: Industrial production of limestone calcined clay cement:

Experience and insights. Green Mater. 7, 15–27 (2018). https://doi.org/10.1680/jgrma.18.00003

16. Atasever, M., Erdoğan, S.T.: Effects of clay type and component fineness on the hydration and properties of limestone calcined clay cement. Materials and Structures/Materiaux et Constructions. 57, (2024). https://doi.org/10.1617/s11527-024-02461-4

17. Scrivener, K., Avet, F., Maraghechi, H., Zunino, F., Ston, J., Hanpongpun, W., Favier, A.: Impacting factors and properties of limestone calcined clay cements (LC3). Green Mater. 7, 3–14 (2018). https://doi.org/10.1680/jgrma.18.00029

18. Matschei, T., Lothenbach, B., Glasser, F.P.: The role of calcium carbonate in cement hydration. Cem. Concr. Res. 37, 551–558 (2007). https://doi.org/10.1016/j.cemconres.2006.10.013

19. Guggenheim, S., & Martin, R. T. Definition of clay and clay mineral: Joint report of the AIPEA nomenclature and CMS nomenclature committees. Clays and Clay Minerals, 43(2), 255–256, (1995).

20. Bergaya, F., Lagaly, G.: Chapter 1 General Introduction: Clays, Clay Minerals, and Clay Science, (2006)

21. Kumari, N., & Mohan, C. Basics of clay minerals and their characteristic properties. In G. M. do Nascimento (Ed.), Clay and clay minerals, (2021).

22. Pourhakkak, P., Taghizadeh, M., Taghizadeh, A., Ghaedi, M.: Adsorbent. In: Interface Science and Technology. pp. 71–210. Elsevier B.V. (2021)

23. Liu, X., Liu, X., Hu, Y.: Investigation of the thermal behaviour and decomposition kinetics of kaolinite. Clay Miner. 50, 199–209 (2015). https://doi.org/10.1180/claymin.2015.050.2.04

24. Alujas, A., Fernández, R., Quintana, R., Scrivener, K.L., Martirena, F.: Pozzolanic reactivity of low grade kaolinitic clays: Influence of calcination

temperature and impact of calcination products on OPC hydration. Appl. Clay Sci. 108, 94–101 (2015). https://doi.org/10.1016/j.clay.2015.01.028

25. Mohammadi, M., Salarirad, M.M.: Dehydroxylation kinetics of alunite. Ind. Eng. Chem. Res. 52, 7333–7340 (2013). https://doi.org/10.1021/ie400127q

26. Küçük, F., Yildiz, K.: The decomposition kinetics of mechanically activated alunite ore in air atmosphere by thermogravimetry. Thermochim. Acta. 448, 107–110 (2006). https://doi.org/10.1016/j.tca.2006.07.003

27. Zhong, Y., Gao, J., Meng, L., Guo, Z.: Phase transformation and non-isothermal kinetics studies on thermal decomposition of alunite. J. Alloys Compd. 710, 182–190 (2017). https://doi.org/10.1016/j.jallcom.2017.03.248

28. Ece, Ö.I., Ekinci, B., Schroeder, P.A., Crowe, D., Esenli, F.: Origin of the Düvertepe kaolin-alunite deposits in Simav Graben, Turkey: Timing and styles of hydrothermal mineralization. Journal of Volcanology and Geothermal Research. 255, 57–78 (2013). https://doi.org/10.1016/j.jvolgeores.2013.01.012

29. Dibowski, G., Neumann, A., Rietbrock, P., Willsch, C., Säck, J.-P., & Funken, K.-H. Der neue Hochleistungsstrahler des DLR – Grundlagen, Technik, Anwendung [Conference presentation]. (2007, June 21).

30. BASF Türk Kimya San. ve Tic. Ltd. Şti. MasterGlenium SKY 608: Yüksek oranda su azaltıcı, süperakışkanlaştırıcı beton katkısı [Technical data sheet]. (2015, October).

31. Kostova, B., Petkova, V., Kostov-Kytin, V., Tzvetanova, Y., Avdeev, G.: TG/DTG-DSC and high temperature in-situ XRD analysis of natural thaumasite. Thermochim. Acta. 697, (2021). https://doi.org/10.1016/j.tca.2021.178863

32. Antoni, M., Baquerizo, L., Matschei, T.: Investigation of ternary mixes made of clinker limestone and slag or metakaolin: Importance of reactive

alumina and silica content. RILEM Bookseries. 10, 545–553 (2015). https://doi.org/10.1007/978-94-017-9939-3_68

33. Huenger, K.J., Sander, I., Zuckow, N.: On the Workability of Mortar and Concrete Mixtures Containing Calcined Clay Blends. In: RILEM Bookseries. pp. 219–227. Springer (2020)

34. Nair, N., Mohammed Haneefa, K., Santhanam, M., Gettu, R.: A study on fresh properties of limestone calcined clay blended cementitious systems. Constr. Build. Mater. 254, (2020). https://doi.org/10.1016/j.conbuildmat.2020.119326

35. ASTM International. Standard test method for flow of hydraulic cement mortar (ASTM C1437-20), (2020).

36. ASTM International. Standard specification for concrete aggregates (ASTM C33/C33M-24a), (2024)

37. ASTM International. Standard test method for flexural strength of hydraulic-cement mortars (ASTM C348-21), (2021).

38. ASTM International. Standard test method for compressive strength of hydraulic-cement mortars (using portions of prisms broken in flexure) (ASTM C349-24), (2024).

APPENDICES

A. Supplementary Data on Raw Material Characterization

Table A.1 Oxide composition of the raw materials

Oxides (wt%)	Clay	Limestone	Gypsum	Clinker
SiO_2	52.45	0.09	2.24	18.25
Al_2O_3	27.81	0.05	0.77	4.94
Fe_2O_3	2.54	0.03	0.50	4.92
CaO	0.54	54.60	32.71	65.43
K_2O	0.78	0.00	0.13	1.11
MgO	0.21	1.14	0.37	1.11
SO_3	2.54	0.08	39.68	1.14
Others	1.13	0.01	0.2	1.2
LOI(*)	12.0	44.0	23.4	1.90

(*) LOI: Loss on ignition. Determined by ASTM D7348

Table A.2 Detailed Gaussian peak-fitting parameters fort he raw clay DTG Curve.

Model	Gaussian				
Equation	y = y0 + A/(w*sqrt(pi/(4*ln(2)))) * exp(-4*ln(2)*(x-xc)^2/w^2)				
Plot	Peak1(Raw)	Peak2(Raw)	Peak3(Raw)	Peak4(Raw)	Peak5(Raw)
y0	0.02522 ± 6.05356E-5	0.02522 ± 6.05356E-5	0.02522 ± 6.05356E-5	0.02522 ± 6.05356E-5	0.02522 ± 6.05356E-5
xc	251.50402 ± 0	501.03803 ± 0	536.71701 ± 0	656.66845 ± 0	739.18979 ± 0
A	0.76263 ± 0.01232	9.25218 ± 0.07044	56.37632 ± 0.08946	10.61127 ± 0.03798	8.83231 ± 0.02405
w	24.36287 ± 0.44318	88.30552 ± 0.38446	114.78088 ± 0.10628	69.93857 ± 0.2377	52.62128 ± 0.14456
R-Square (COD)	0.99181				
Adj. R-Square	0.99181				

B. Temperature Profiles During Solar Calcination

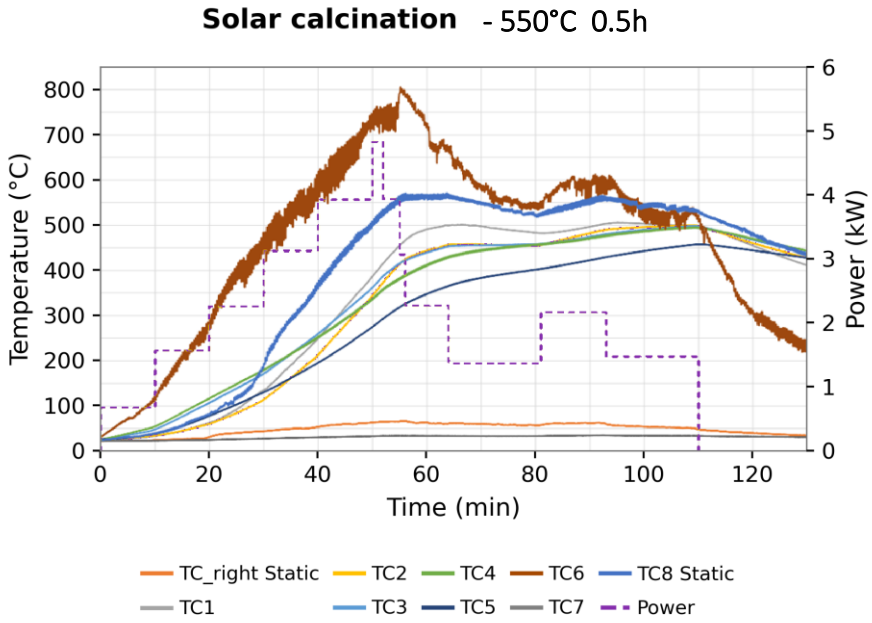

Figure B.1. Temperature profiles solar calcination at 550 °C for holding time of 0.5.

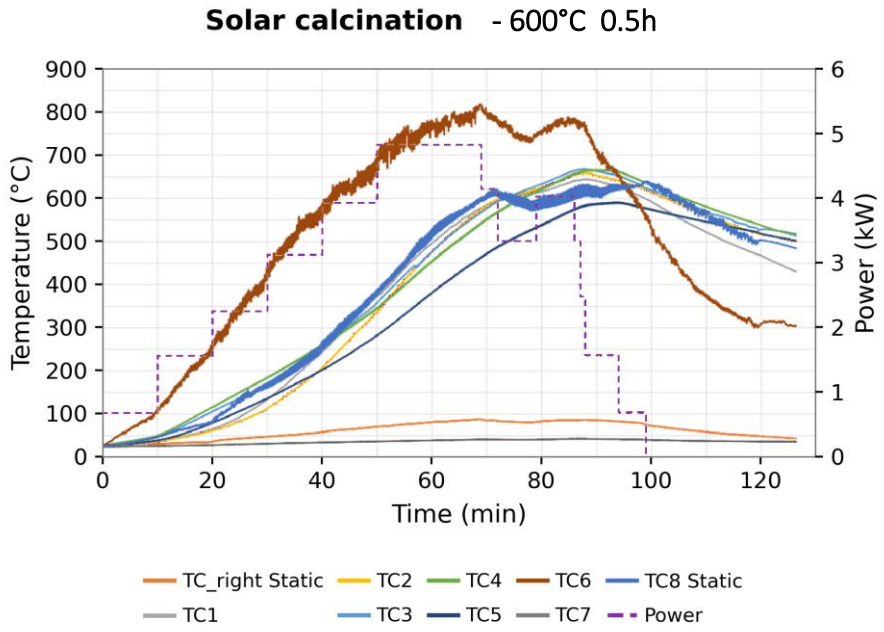

Figure B.2. Temperature profiles solar calcination at 600 °C for holding time of 0.5.

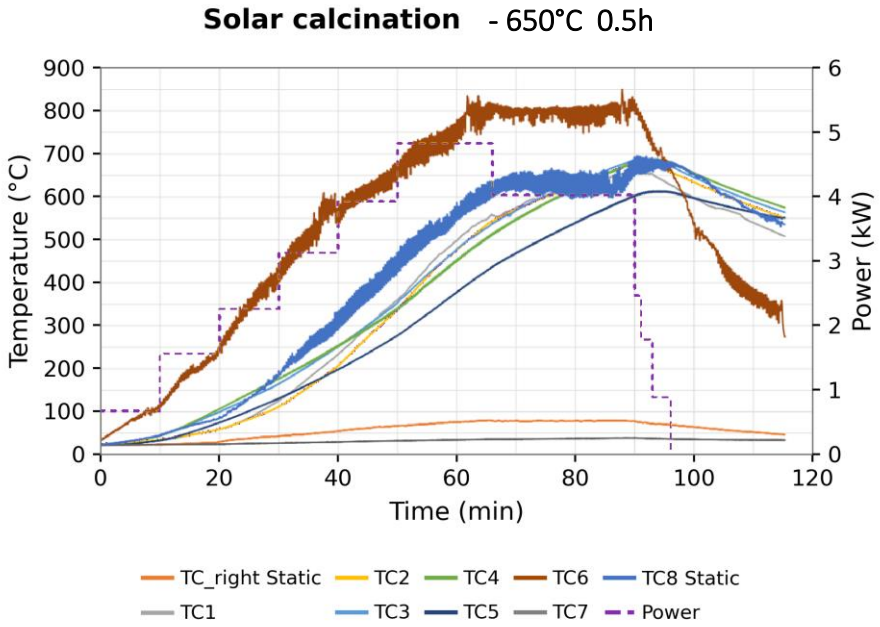

Figure B.3. Temperature profiles solar calcination at 650 °C for holding time of 0.5.

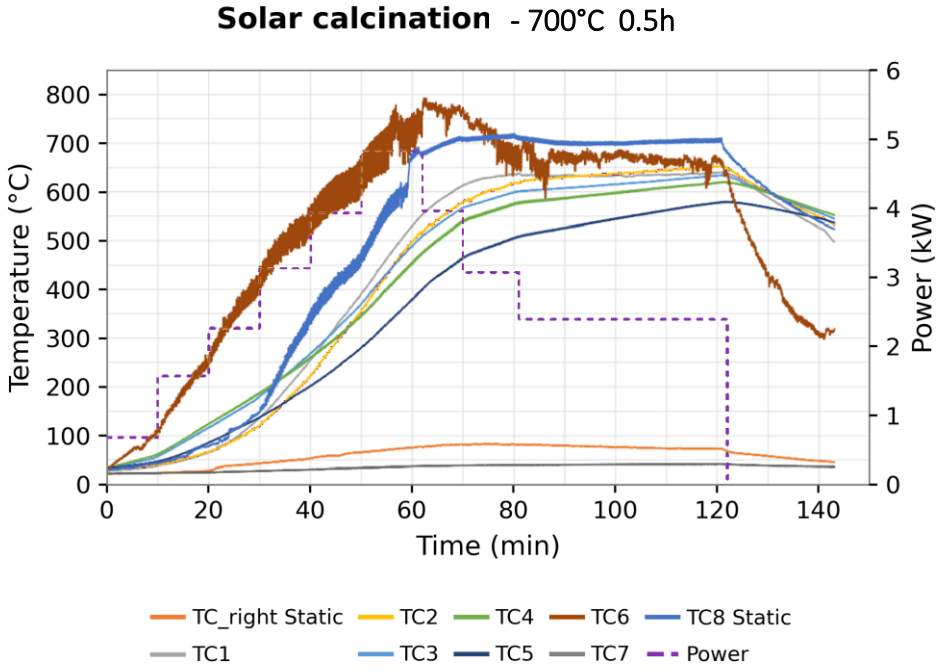

Figure B.4. Temperature profiles solar calcination at 700 °C for holding time of 0.5.

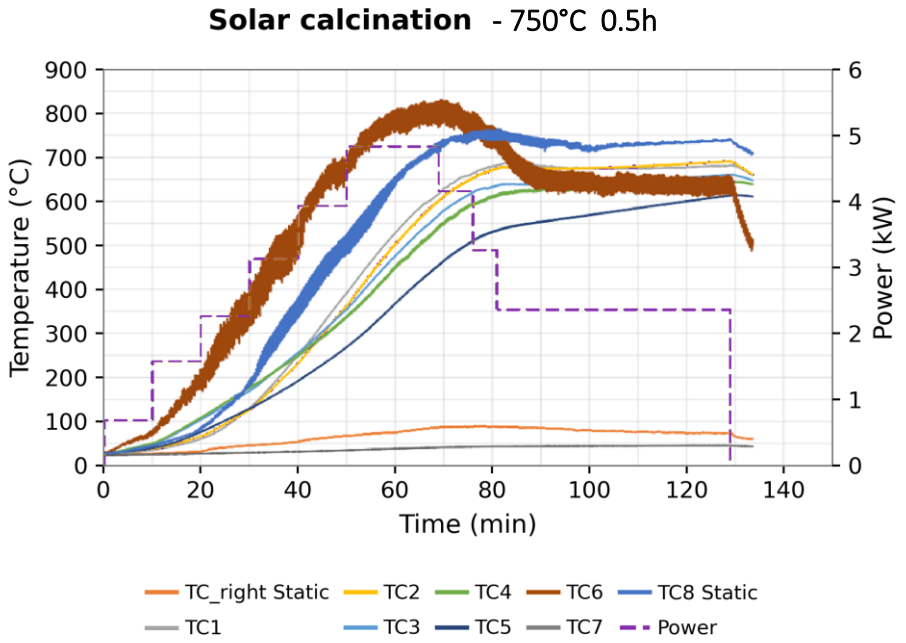

*Fig*ure B.5. Temperature profiles solar calcination at 750 °C for holding time of 0.5.

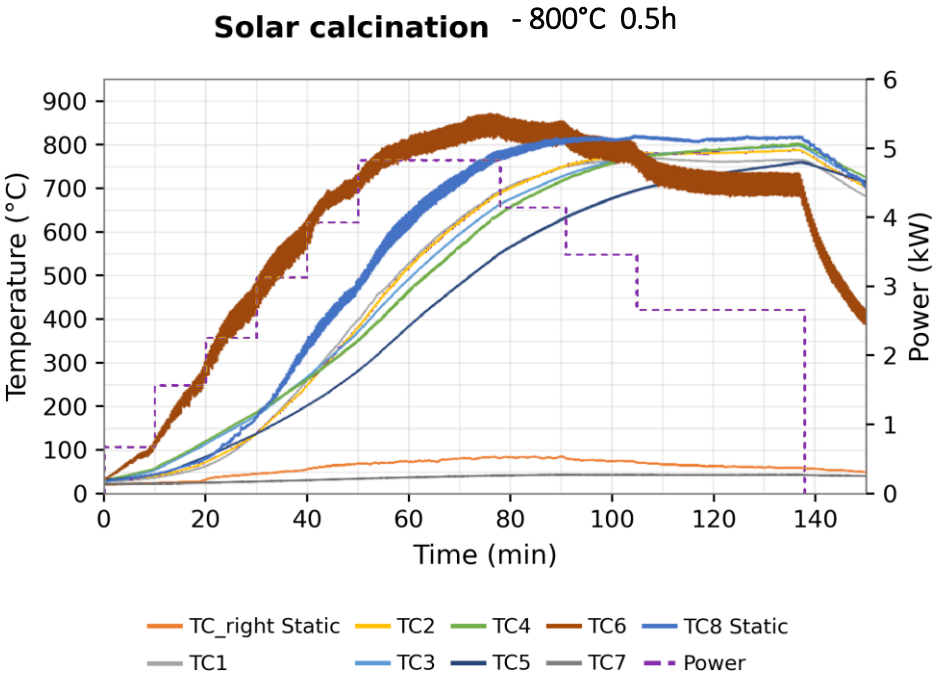

Figure B.6. Temperature profiles solar calcination at 800 °C for holding time of 0.5.

C. Temperature Profiles During Furnace Calcination

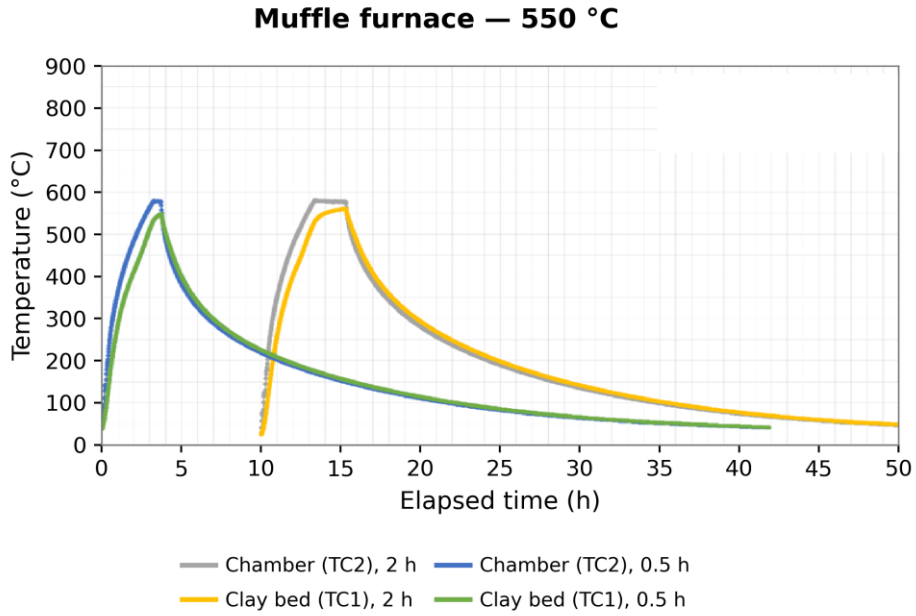

Figure C.1. Temperature profiles furnace calcination at 550 °C for holding times of 0.5 and 2 h.

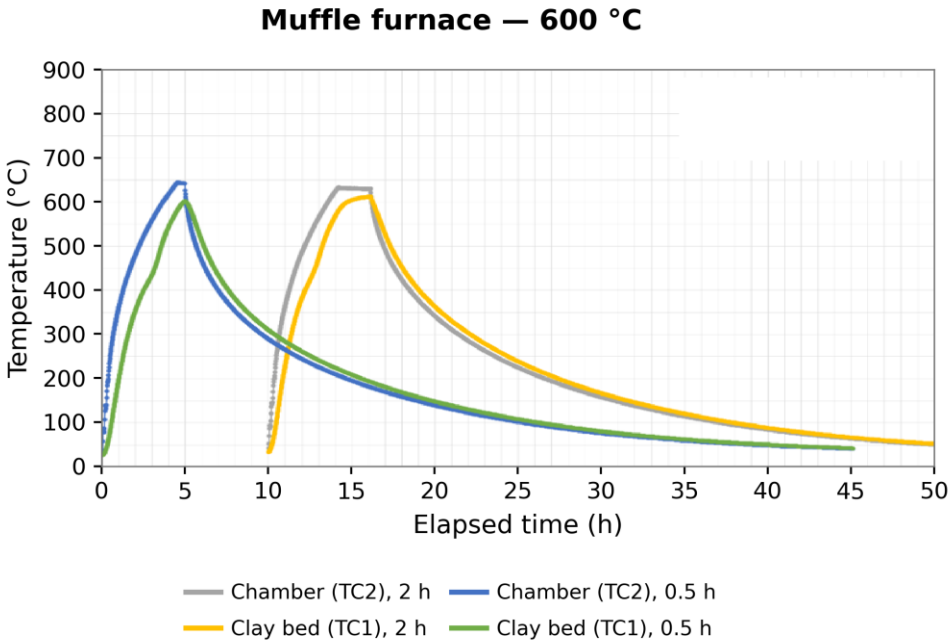

Figure C.2. Temperature during furnace calcination at 600 °C for holding times of 0.5 and 2 h.

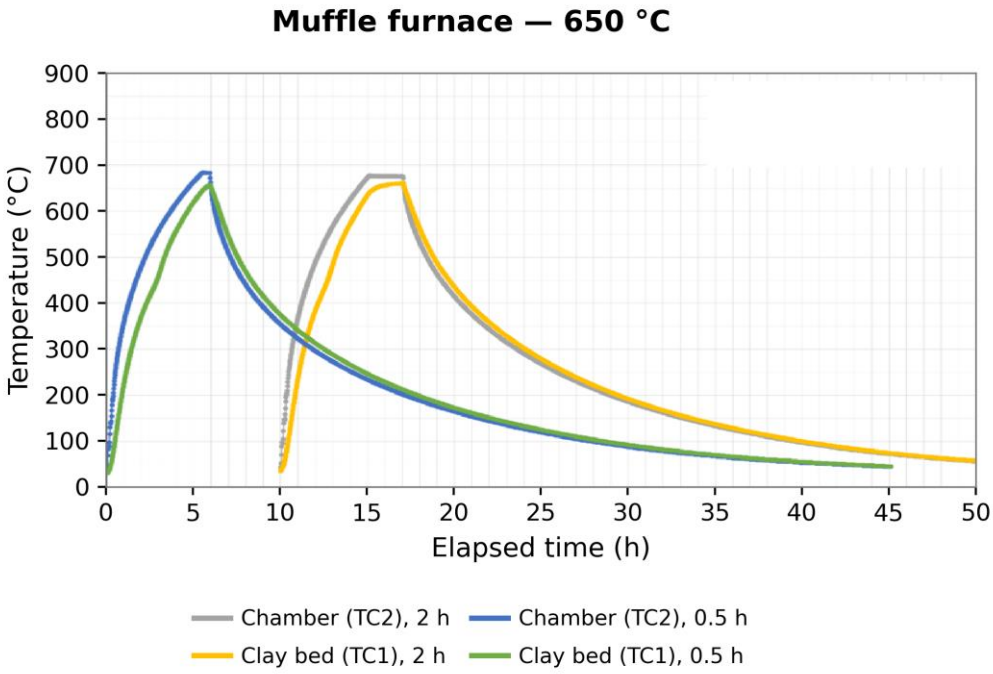

Figure C.3. Temperature during furnace calcination at 650 °C for holding times of 0.5 and 2 h.

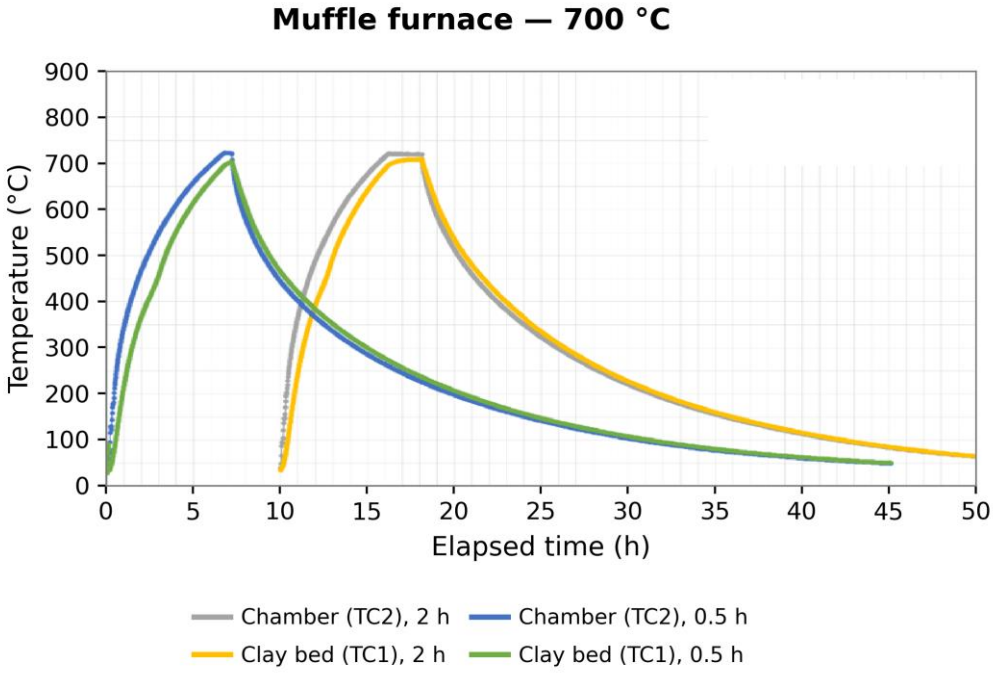

Figure C.4. Temperature during furnace calcination at 700 °C for holding times of 0.5 and 2 h.

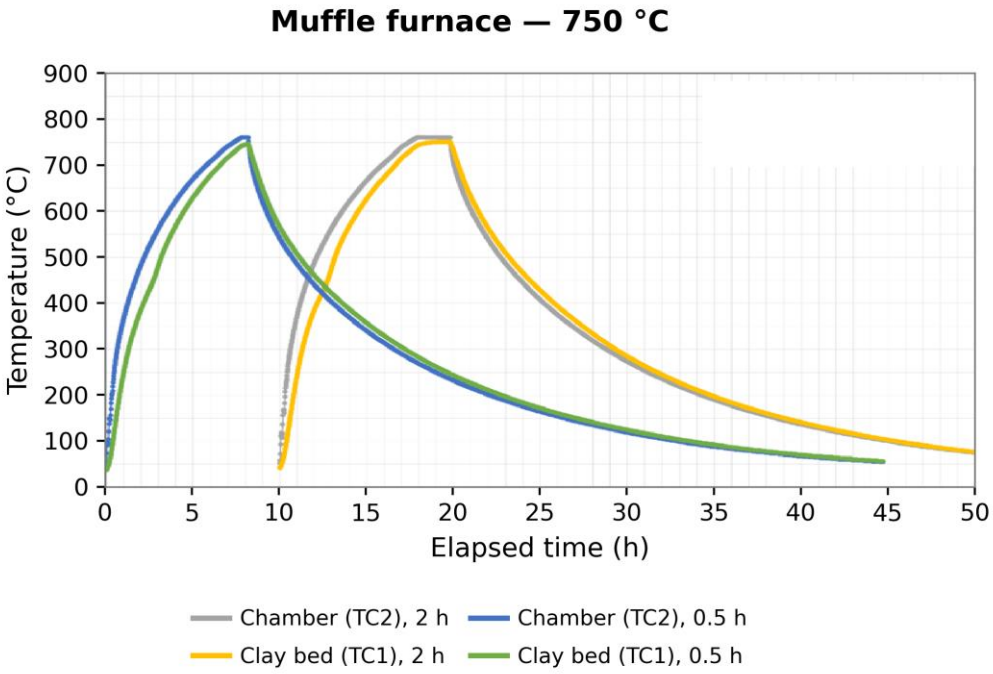

Figure C.5. Temperature profiles furnace calcination at 750 °C for holding times of 0.5 and 2 h.

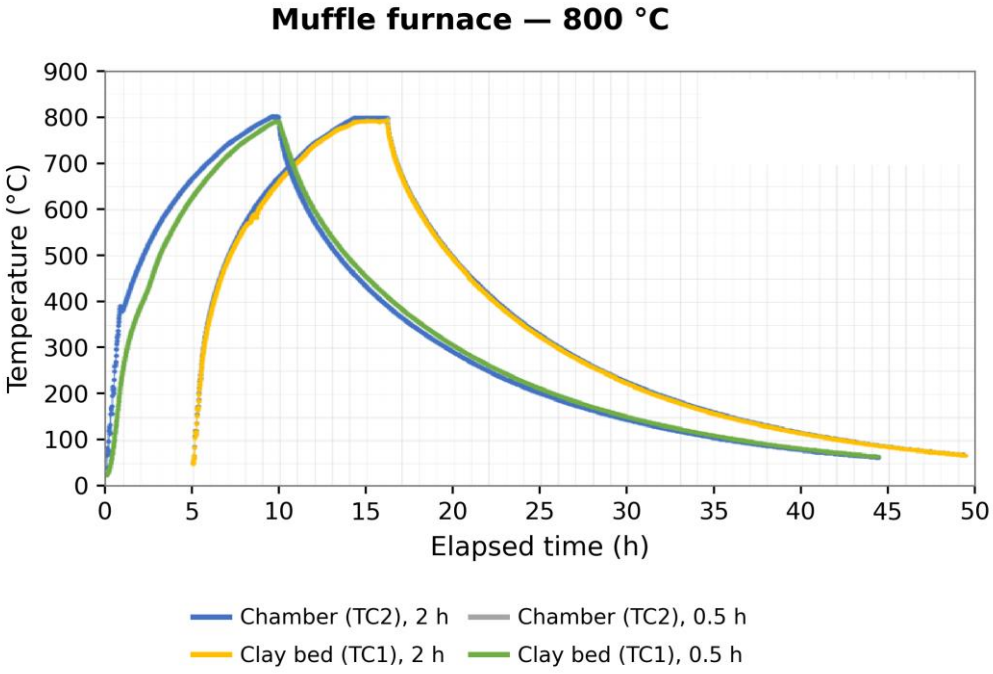

Figure C.6. Temperature profiles furnace calcination at 800 °C for holding times of 0.5 and 2 h.